

Leveraging Secondary Storage to Simulate Deep 54-qubit Sycamore Circuits

Edwin Pednault^{*1}, John A. Gunnels¹, Giacomo Nannicini¹, Lior Horesh¹, and Robert Wisnieff¹

¹IBM T.J. Watson Research Center, Yorktown Heights, NY

Abstract

In a recent paper, we showed that secondary storage can extend the range of quantum circuits that can be practically simulated with classical algorithms. Here we refine those techniques and apply them to the simulation of Sycamore circuits with 53 and 54 qubits, with the entanglement pattern ABCDCDAB that has proven difficult to classically simulate with other approaches. Our analysis shows that on the Summit supercomputer at Oak Ridge National Laboratories, such circuits can be simulated with high fidelity to arbitrary depth in a matter of days, outputting all the amplitudes.

1 Introduction

There has been tremendous progress in the construction of quantum computers with superconducting qubits [4]. As the hardware progresses, it is increasingly difficult to classically simulate the circuits that can be executed on existing chips, a crucial task to – among other things – verify that the degree to which hardware is behaving as expected. The literature contains several papers that discuss this task and that have been published or posted online in the past two years [14, 3, 7, 10, 5, 11, 16, 6, 17, 8, 18]. Here we extend the analysis on the use of secondary storage initially reported in our previous work [14]. As we argued in that paper, secondary storage can extend the computational reach of supercomputers for the simulation of quantum circuits — an idea initially suggested by [9]. We estimate that on the Summit supercomputer at Oak Ridge National Laboratories, secondary storage allows the simulation of 53- and 54-qubit Sycamore circuits [15] with high fidelity to arbitrary depth. The Sycamore circuits are a direct descendant of the “universal random circuits” described in [2]. In particular, for 20 cycles of the entanglement pattern ABCDCDAB, which is specifically designed to challenge classical simulation algorithms, we estimate that the computations would take approximately two and a half days. While we did not carry out these computations, we provide a detailed description of the proposed simulation strategy as well as the time estimation methodology, which is based on published results and on internal benchmarks. The main building blocks of our approach are the same as those that we discussed in [14], namely: exploitation of separable gates via a hyperedge representation of the tensor network; allowing contractions between non-adjacent tensors; tensor slicing; and sporadic read/write operations to access/store slices of the quantum state in secondary storage.

The rest of this paper is organized as follows. In Sect. 2 we provide a review of the main building blocks of our simulation strategy. Sect. 3 describes the class of circuits studied in this work. Sect. 4 gives a detailed explanation of the simulation strategy and its use of secondary storage. Sect. 5 concludes the

^{*}Corresponding author; pednault@us.ibm.com

paper by estimating the time required by the proposed simulations, and discussing the methodology to compute such estimates. The Appendix contains a detailed listing of the operations performed by the proposed simulation strategy.

2 Brief overview of tensor contraction deferral

The simulation algorithm that we propose is based on the idea of partitioning a quantum circuit into subcircuits that can be simulated independently, at the expense of extra bookkeeping to account for entanglement between subcircuits. We ensure that the final results are correct by appropriately recombining the different subcircuits and, in some sense, “resolving” the entanglement. Rather than insisting that all subcircuits reside in primary storage, i.e., RAM, we allow for storing the results of some of the calculations on secondary storage, e.g., disk. This is particularly effective when combined with slicing techniques, which further partition the quantum state by iteratively fixing the value of some of the indices in the tensor network.

We now give a brief overview of the main components of our simulation strategies; for details and several examples, we refer the reader to our earlier work [14]. A *tensor* is a multilinear map with a set of indices to address its elements. In the context of this paper, each index takes value in $\{0, 1\}$. As discussed in [14], a *tensor network* is a hypergraph $G = (V, E)$ such that each node is associated with a tensor and each hyperedge with an index of the adjacent tensors. Hyperedges between nodes represent shared indices that must be summed over. A summation over shared indices is called a *contraction*. A tensor $A_{i_1, \dots, i_m, j_1, \dots, j_m}$ is *diagonal* if it is nonzero only if $i_k = j_k$ for $k = 1, \dots, m$. A tensor is *separable* if it can be obtained from a diagonal tensor with a permutation, i.e., there exist functions f_1, \dots, f_m such that $A_{f_1(j_1, \dots, j_m), \dots, f_m(j_1, \dots, j_m), j_1, \dots, j_m}$ is diagonal. Our hypergraph representation is designed to take advantage of separable tensors, since the computational resources necessary to perform a contraction between several tensors can be significantly reduced in the presence of indices shared among multiple tensors — represented by hyperedges. Given a quantum circuit, we can construct a tensor network by letting the gates correspond to tensors, and the qubit lines roughly correspond to the indices (i.e. edges and hyperedges). To simulate large circuits, we rely extensively on *contraction deferral* and *tensor slicing*, which we describe more fully below.

Contraction deferral is a technique first introduced in [1]. Its use in large-scale simulations was pioneered in [14]. Contraction deferral is defined as the contraction of arbitrary sets of (potentially non-adjacent) tensors in the tensor network; this is in contrast with the adjacent contraction discussed in the seminal work [12] and in several subsequent papers, e.g., [3]. A deferred contraction performs the usual summation over shared indices (i.e., edges interior to the set being contracted), and applies an outer product to the non-shared indices. As it is a generalization of the traditional adjacent contraction, contraction deferral opens up new simulation strategies that can lead to reduced memory requirements. In particular, we partition the tensor network into sub-hypergraphs corresponding to subcircuits, each of which includes fewer qubits than the initial circuit. Within each circuit we perform computations following the so-called “Schrödinger approach” [1], i.e., evolving the full quantum state of the subcircuit by applying layers of gates one at a time. To do so, we must use contraction deferral whenever we apply tensors corresponding to entangling gates between different subcircuits.

Tensor slicing is the idea of iterating over several instances of a circuit in which certain hyperedges (i.e., tensor indices) are fixed to one of their possible values. While this does not necessarily reduce the number of operations to be performed, it allows reordering the computations so that they take place in ways that are potentially more efficient. This is particularly crucial when using secondary storage, which is slower than primary storage and must therefore be used sparingly; with tensor slicing, we reorganize the calculations so that only a few selected slices (rather than full tensors) reside in primary storage at any given time. Our scheme extends the simulation strategy in [9]: we choose a set of indices, slice

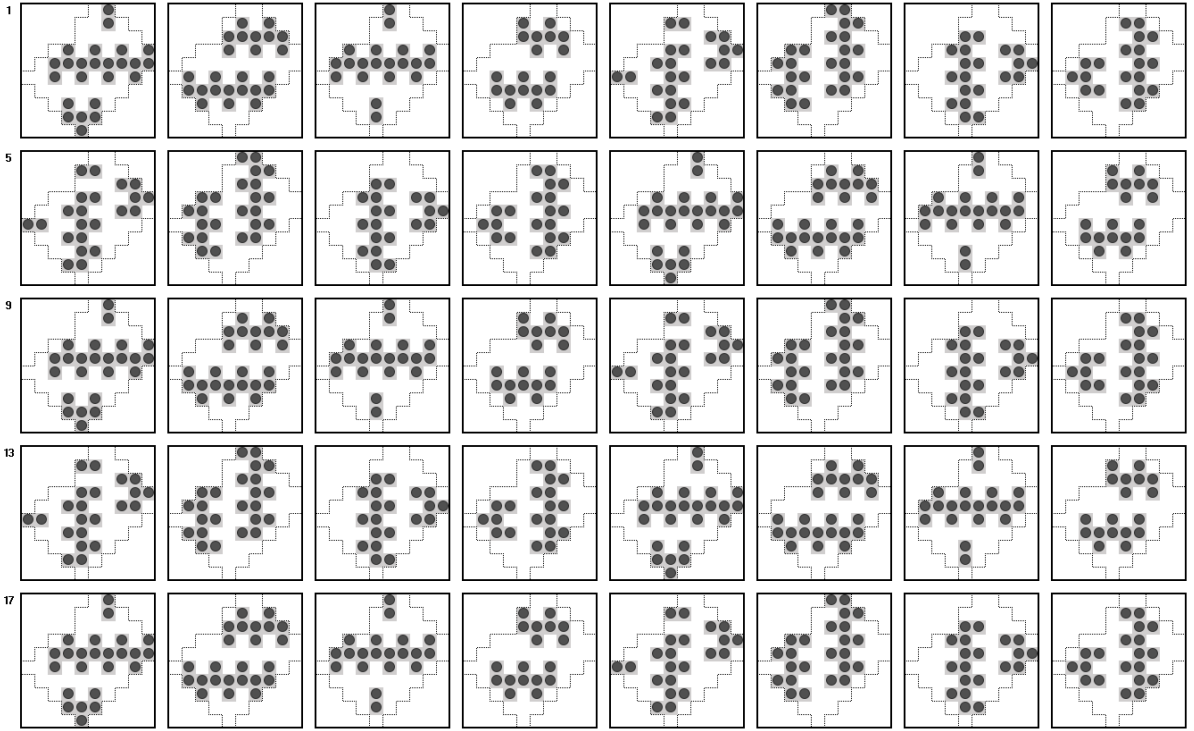


Figure 1: Gate pattern for a 20-cycle, 53-qubit, Sycamore ABCDCDAB circuit. Single-qubit gates are merged into their neighboring two-qubit gates, and the two-qubit gates in each cycle are partitioned into two layers for illustration purposes to make the individual gates easy to identify. These transformations result in the 40-layer circuit depicted. Dots and shading are used to identify which pairs of qubits are being operated upon.

them by looping over every possible combination of their values, and use a superset of those qubits to efficiently organize and address information located in secondary storage.

3 Sycamore circuits

A recent paper [15] describes a new class of random quantum circuits consisting of alternating layers of single-qubit gates and two-qubit gates. The combination of a layer of single-qubit gates followed by a layer of two-qubit gates is referred to in [15] as a *cycle*. Our paper discusses the classical simulation of circuits of this class; hence, we describe them here in more detail. Gates are applied to all qubits in each single-qubit gate layer, and to almost all qubits in each two-qubit gate layer. The two-qubit gates are all non-diagonal, non-separable and their unitary representation varies as a function of both the location of the gate within the qubit layout, and the depth at which the gate is applied in the circuit. The former reflects variations in gate tuning, while the latter reflects variations in pulse synchronization over time. Circuits consist of several cycles of single-qubit gates followed by two-qubit gates, together with a final layer of single-qubit gates. The single-qubit gates are randomly selected from the set $\{\sqrt{X}, \sqrt{Y}, \sqrt{W}\}$.

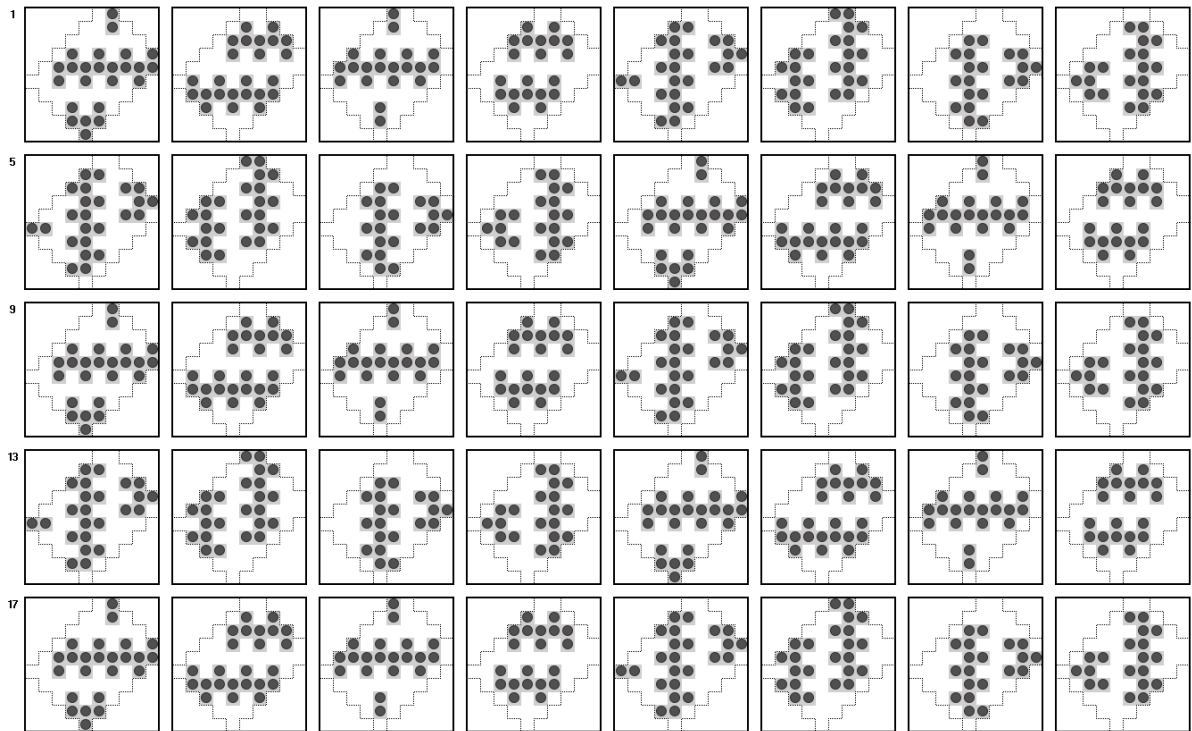


Figure 2: Gate pattern for a 20-cycle, 54-qubit, Sycamore ABCDCDAB circuit. Single-qubit gates are merged into their neighboring two-qubit gates, and the two-qubit gates in each cycle are partitioned into two layers for illustration purposes to make the individual gates easy to identify. These transformations result in the 40-layer circuit depicted. Dots and shading are used to identify which pairs of qubits are being operated upon.

The two-qubit gates implement the following unitary:

$$\begin{bmatrix} 1 & 0 & 0 & 0 \\ 0 & e^{i(\Delta_++\Delta_-)} \cos \theta & -ie^{i(\Delta_+-\Delta_{-,off})} \sin \theta & 0 \\ 0 & -ie^{i(\Delta_++\Delta_{-,off})} \sin \theta & e^{i(\Delta_+-\Delta_-)} \cos \theta & 0 \\ 0 & 0 & 0 & e^{i(2\Delta_+-\phi)} \end{bmatrix}, \quad (1)$$

where θ and ϕ are nominally 90° and 30° , respectively, and where Δ_+ , Δ_- , and $\Delta_{-,off}$ are detuning terms. For simulation purposes, all single-qubit gates can be aggregated with neighboring two-qubit gates, yielding an equivalent circuit consisting of (potentially unique) two-qubit gates only. The method for selecting single-qubit gates ensures that these two-qubit unitary operations are also randomized. The difficulty of simulation is therefore determined entirely by the pattern of two-qubit gates in the circuit.

Figs. 1 and 2 illustrate the “ABCDCDAB” patterns of two-qubit gates used in the 53- and 54-qubit random circuits described in [15] to test the Sycamore quantum device. This pattern is intentionally devised to make the resulting circuits difficult to simulate classically. For illustration purposes, each cycle of two-qubit gates is depicted as two layers in the figures, so that we can unambiguously indicate the pairs of qubits involved in each gate operation (i.e., vertical pairs versus horizontal pairs). Thus, the first two layers of two-qubit gates illustrated correspond to the “A” cycle, the next two layers to the “B” cycle, and so on. In this representation, the first row corresponds to an “ABCD” sequence of cycles, the second row corresponds to a “CDAB” sequence of cycles, and the five rows illustrated in Figs. 1 and 2 correspond to the 20-cycle circuits generated according to the ABCDCDAB rules described in [15].

4 Proposed simulation strategy

In [9] the authors suggest that solid-state disk, or more generally secondary storage, could be used to supplement main memory in order to simulate circuits whose quantum states are too large to store in main memory alone. In [14], we combined our in-memory methods with those of [9], describing a viable computation scheme that exploits secondary storage to simulate deeper circuits than was thought possible. We now apply the approach discussed in [14] to 53- and 54-qubit Sycamore circuits, showing in this section a computation scheme that allows their simulation on an existing supercomputer, Summit. The cost of such a scheme is discussed in Sect. 5.

The simulation method in [9] can be seen as a tensor slicing approach. Qubits (and the corresponding tensor indices) are divided into “global” qubits, which are sliced and used to address across processing nodes, and “local” qubits, corresponding to tensor indices used to address tensor slices stored on each processing node. In [9], circuits are partitioned so that all gates within a subcircuit can be applied to the local slice of the quantum state, without communicating quantum state information among processing nodes. Such zero-communication updates of a local quantum state are possible when all non-diagonal gates in a subcircuit are applied to local qubits only. They are also possible for a handful of additional circumstances described in [9]. In effect, circuits are partitioned by selecting different subsets of local qubits and analyzing which gates can be applied to them without communication. This determines the subcircuits. During simulation, communication between processing nodes occurs only when the simulation switches from one subcircuit to another. When a communication phase takes place, the memory layout of quantum state tensors is reorganized so that different global and local qubits (i.e., tensor indices) are selected, according to the subcircuits that have to be simulated in the subsequent phase.

The in-memory method that we presented in [14] considers circuit partitionings in which the resulting tensors either fit in available aggregate primary memory in their entirety, or their slices can be computed using available primary memory (using other tensors already computed and stored in primary

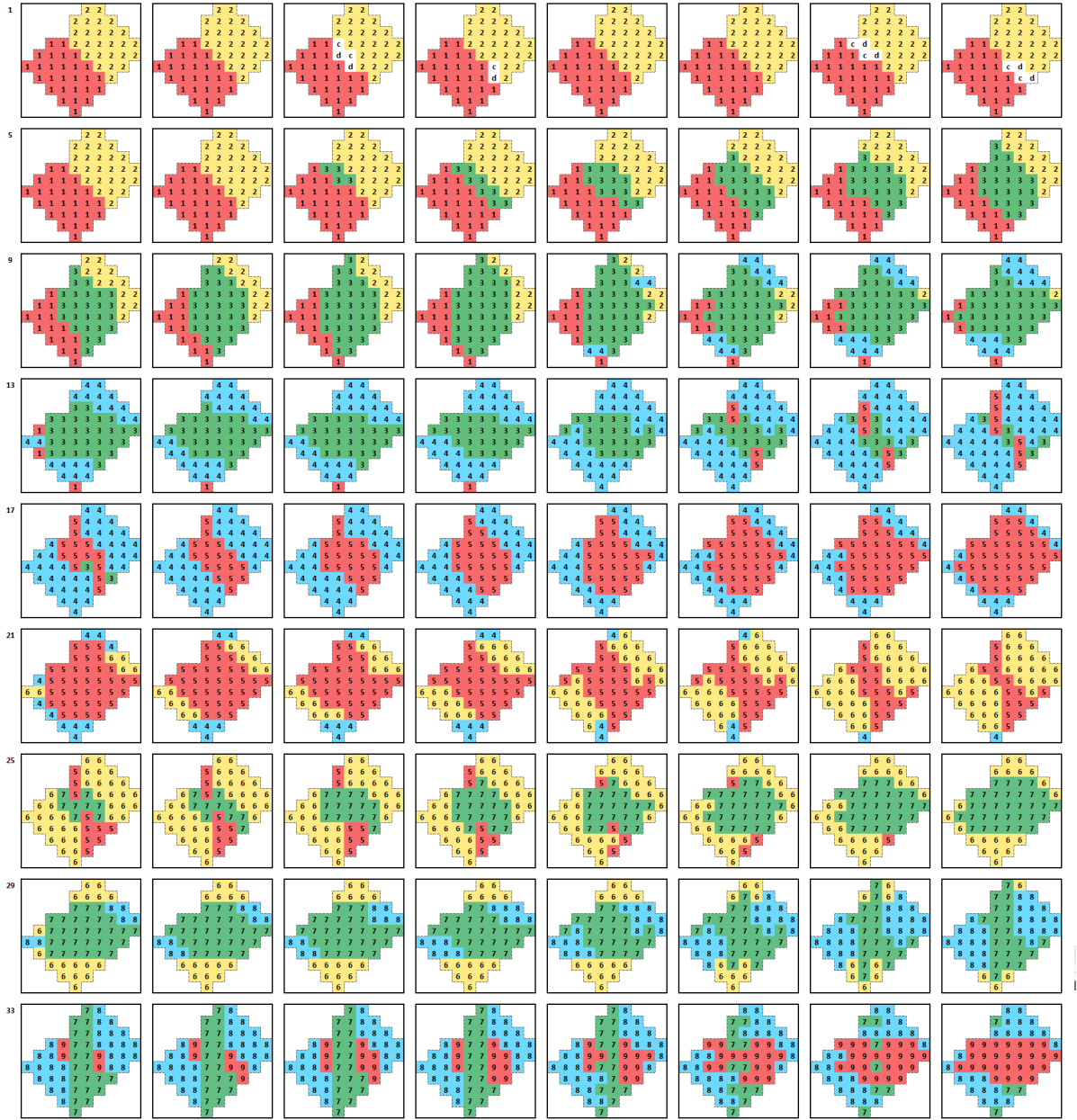


Figure 3: Partitioning of a 36-cycle, 53-qubit, Sycamore ABCDCDAB circuit to leverage secondary storage. Numbers and colors are used to indicate regions of gates within the circuit that are grouped together to form subcircuits, and also to refer to specific subcircuits in the text. Contraction deferral is applied to the gates labeled “cd.”

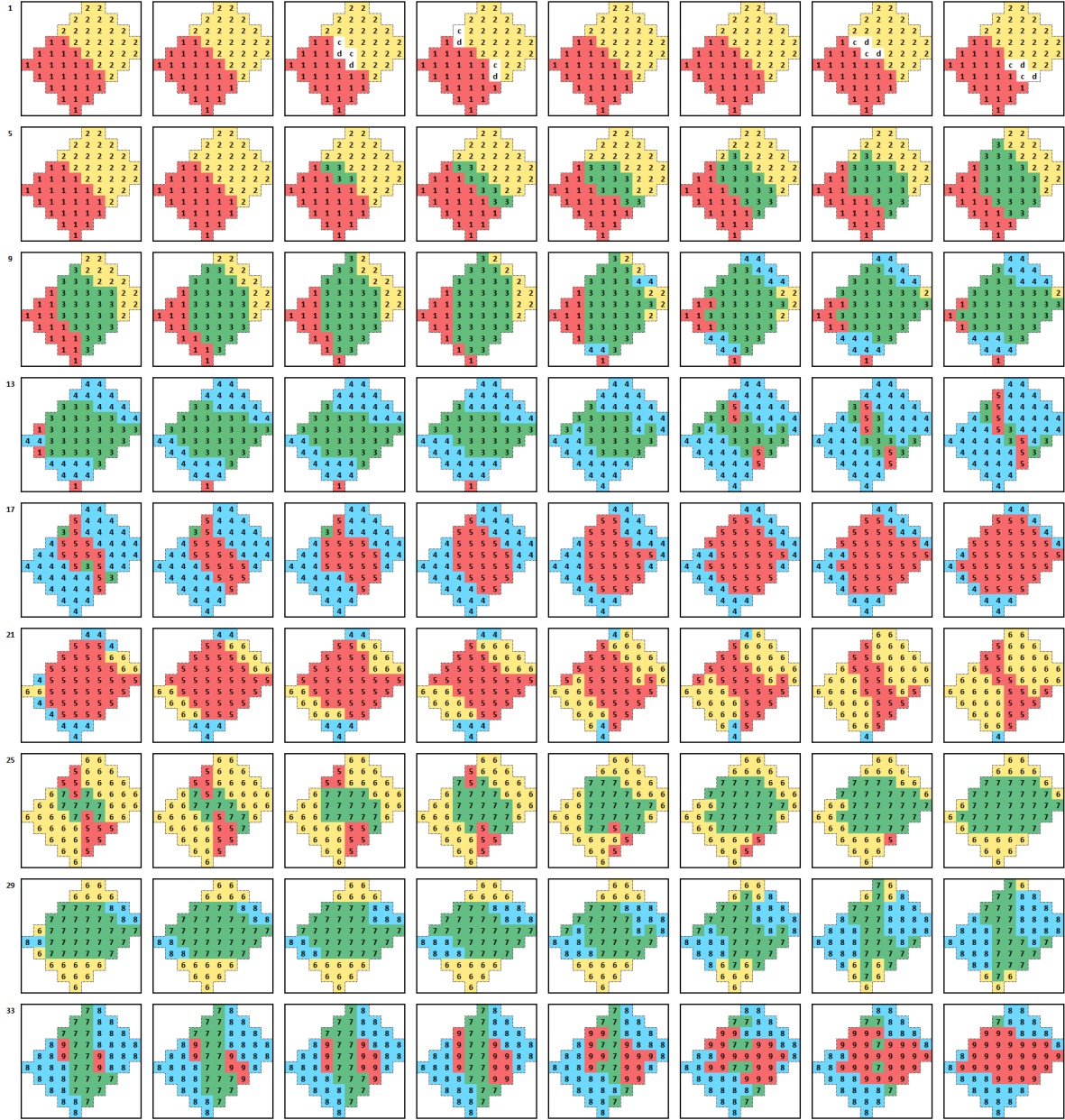


Figure 4: Partitioning of a 36-cycle, 54-qubit, Sycamore ABCDCDAB circuit to leverage secondary storage. Numbers and colors are used to indicate regions of gates within the circuit that are grouped together to form subcircuits, and also to refer to specific subcircuits in the text. Contraction deferral is applied to the gates labeled “cd.”

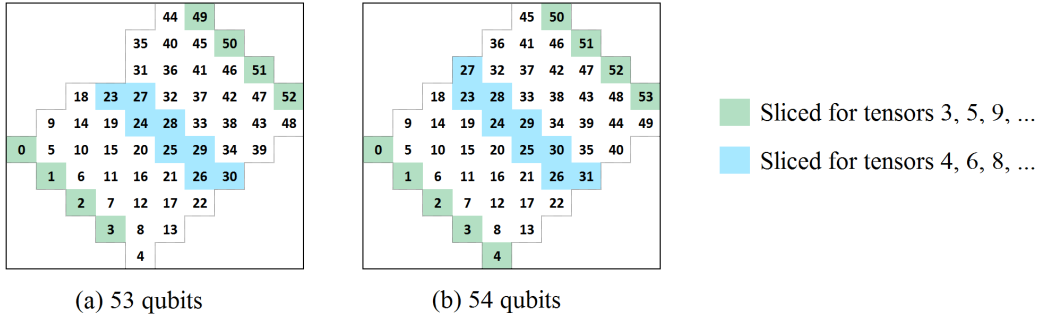


Figure 5: Qubit numbering scheme and first-level tensor slicing strategy for 53- and 54-qubit Sycamore circuits.

memory). With this approach, the resulting tensors and/or their slices will generally be larger than the primary memories of individual processing nodes; this represents a difference between [14] and [9].

As discussed in [14], we combine the zero-communication strategies of [9] with our own tensor partitioning strategy to leverage secondary storage when quantum states are too large to fit in aggregate primary memory. Because secondary storage is typically orders of magnitude slower than main memory, the viability of using it depends on the extent to which the number of read/write cycles can be minimized or overlapped with computation. To this end, we first employ the in-memory methods of [14], aiming to maximize the number of gates that can be simulated using available aggregate memory; the resulting quantum state is calculated in slices and written to secondary storage. The partitioning methods discussed in [9] can then be applied to the remaining gates in the circuit, setting the number of “local” qubits according to the size of aggregate memory, rather than the memory sizes available on individual processing nodes. This increases the size of the resulting tensor slices, allowing the application of many more gates to the local quantum state before additional secondary storage read/write cycles are needed. The resulting subcircuits can be further partitioned into sub-subcircuits, using the methods of [9], to minimize internode communication in the overall calculations. We now provide details about these partitionings for the specific circuits studied in this paper.

Figs. 3 and 4 illustrate the first level of circuit partitioning for 36-cycle Sycamore ABCDCDAB circuits with 53 and 54 qubits, respectively. In this first phase, we use the in-memory methods of [14] to simulate the subcircuits 1 and 2 illustrated in these figures, performing tensor contraction deferral on the gates labeled “cd.” The outer-most qubits of the resulting tensors are used as “global” qubits, with the corresponding slices contracted in order to allow the simulation of subcircuit 3, slice by slice. Each resulting slice for subcircuit 3 is written to disk. Fig. 5 illustrates the “global” qubits that are sliced in this first phase of simulation. In the case of the 53-qubit circuit, qubits 0–3 and 49–52 are sliced in the simulation of subcircuit 3; for the 54-qubit circuit, qubits 0–4 and 50–53 are sliced.

In the second phase, qubits 23–30 are sliced for the 53-qubit circuit and qubits 23–31 are sliced for the 54-qubit circuit. In both cases, the following steps are performed for each slice: the slice is read from disk, the gates in subcircuit 4 shown in Figs. 3 and 4 for the respective circuits are applied, and the slice is written back to disk.

This process is repeated for each subsequent subcircuit, with the choice of sliced qubits alternating between those used for subcircuit 3 and those used for subcircuit 4. Specifically, for subcircuits 5, 7 and 9, in the 53-qubit circuit we slice qubits 0–3 and 49–52, while in the 54-qubit circuit we slice qubits 0–4 and 50–53. For subcircuits 6 and 8, in the 53-qubit circuit we slice qubits 23–30, while in the 54-qubit circuit we slice qubits 23–31. As with subcircuit 4, slices are read from disk, processed, and then written back to disk.

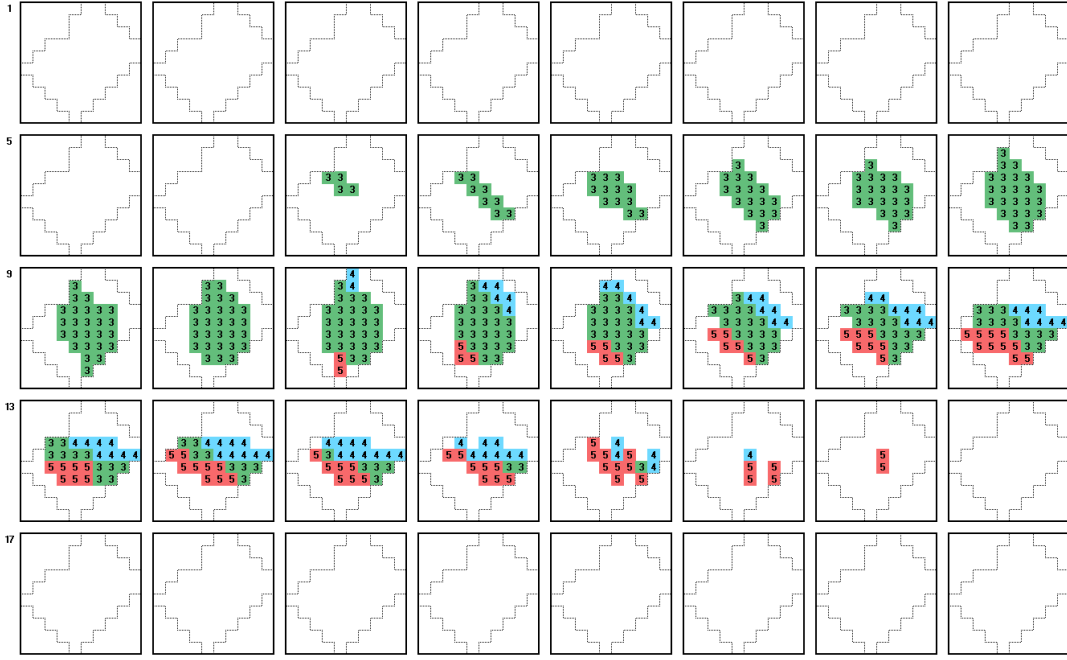


Figure 6: Partitioning of subcircuit 3 to minimize all-to-all communication for the 20-cycle, 53-qubit Sycamore circuit shown in Fig. 1.

To ensure that we efficiently transfer data to/from secondary storage, we organize the data on secondary storage as 2^{16} logical files for the 53-qubit circuit, and 2^{18} logical files for the 54-qubit circuit. In the case of the 53-qubit circuit, files are indexed by the values of qubits 0–3, 23–30, and 49–52; each logical file contains 2^{37} complex amplitudes corresponding to qubits 4–22 and 31–48. In the case of the 54-qubit circuit, files are indexed by the values of qubits 0–4, 23–31, and 50–53; each logical file contains 2^{36} complex amplitudes corresponding to qubits 5–22 and 32–49. Thus, in the first phase of simulation for the 53-qubit circuit (i.e., the phase in which tensor 3 is written to disk), we write 256 logical files to secondary storage for each of the 256 values of qubits 0–3 and 49–52 that are being sliced; these files correspond to the 256 possible values of qubits 23–30. For 54-qubit circuits, 512 logical files are written to secondary storage for each of the 512 values of qubits 0–4 and 50–53 that are being sliced; these files correspond to the 512 possible values of qubits 23–31.

In the second phase of simulation of the 53-qubit circuit (i.e., the phase in which subcircuit 4 is simulated), for each of the 256 values of qubits 23–30 that are being sliced, we read 256 logical files from secondary storage, corresponding to the 256 possible values of qubits 0–3 and 49–52. Once these 256 files of amplitudes are loaded into memory, we apply the gates in subcircuit 4 and write each updated slice back to storage. Similarly, for the 54-qubit circuit, for each of the 512 values of qubits 23–31 that are being sliced, we read 512 logical files from secondary storage, corresponding to the 512 possible values of qubits 0–4 and 50–53. Updated slices are written back to secondary storage as 512 files of amplitudes. These access patterns are repeated for each subsequent phase of processing. The above approach guarantees that individual logical files are always read or written in their entirety, and they are never read or written multiple times in a single read or write cycle. Access overhead per read/write cycle is thereby minimized.

The above slicing strategy is designed to minimize the number of disk accesses by maximizing the number of “local” qubits employed in each disk slice, which is 45 qubits for both the 53- and the 54-qubit circuit. As discussed earlier, the slicing methodology in [9] is applied recursively to these 45-qubit

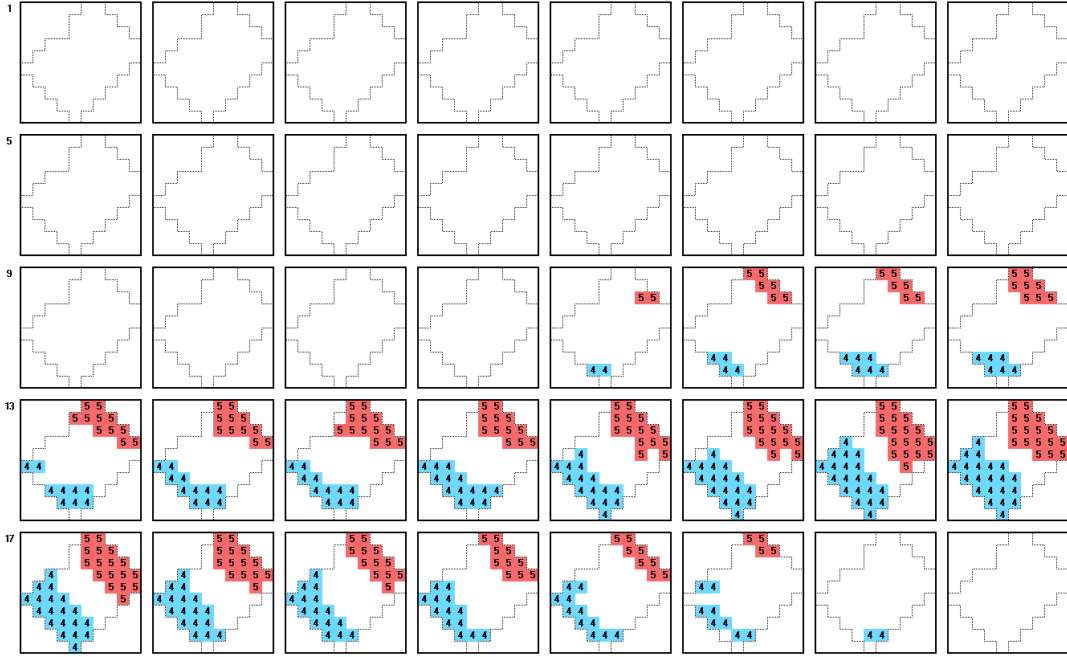


Figure 7: Partitioning of subcircuit 4 to minimize all-to-all communication for the 20-cycle, 53-qubit Sycamore circuit shown in Fig. 1.

slices, to minimize the number of all-to-all communication steps that must be performed in order to simulate subcircuits 3–9, shown in Figs. 3 and 4. Figs. 6–11 illustrate these recursive partitionings for tensors 3, 4, and 5 in the case of 20-cycle circuits. These partitionings correspond to slicing an additional 13 qubits (i.e., in addition to the qubits sliced for disk access purposes), in order to distribute work across 4096 nodes and across each pair of IBM Power 9 sockets within those nodes. We employ a socket-level slicing strategy to enable each socket to work independently, and to avoid Non-Uniform Memory Access (NUMA) overhead when memory accesses cross socket boundaries.

As shown in Figs. 6 and 9, subcircuit 3 is recursively partitioned into three sub-subcircuits, labeled 3, 4, and 5. For the 53-qubit circuit, the sub-subcircuit labeled 3 is sliced on qubits 4–10 and 43–48, and for the 54-qubit circuits we slice qubits 5–10 and 43–49. These specific qubits are selected so that the corresponding slices of tensors 1 and 2, which are small, can be pre-distributed across sockets; this way the contractions needed to start simulating subcircuit 3 can be performed in-place without communication. For 53-qubit circuits, the sub-subcircuit labeled 4 is sliced on qubits 4–16, and, for 54-qubit circuits, on qubits 5–17. This redistribution requires an all-to-all exchange of amplitudes across sockets. For 53-qubit circuits, the sub-subcircuit labeled 5 is sliced on qubits 36–48, and, for 54-qubit circuits, on qubits 37–49, again requiring all-to-all communication.

As shown in Figs. 7 and 10, subcircuit 4 is recursively partitioned into two sub-subcircuits labeled 4 and 5. For 53-qubit circuits, the sub-subcircuit labeled 4 is sliced on qubits 40–52, and for 54-qubit circuits on qubits 41–53. The sub-subcircuit labeled 5 is sliced on qubits 0–12 for both 53- and 54-qubit circuits.

As shown in Figs. 8 and 11, subcircuit 5 is recursively partitioned into two sub-subcircuits labeled 5 and 6. For 53-qubit circuits, the sub-subcircuit labeled 5 is sliced on qubits 36–48, and, for 54-qubit circuits, on qubits 37–49. The sub-subcircuit labeled 6 is sliced on qubits 4–16 for 53-qubit circuits, and on qubits 5–17 for 54-qubit circuits.

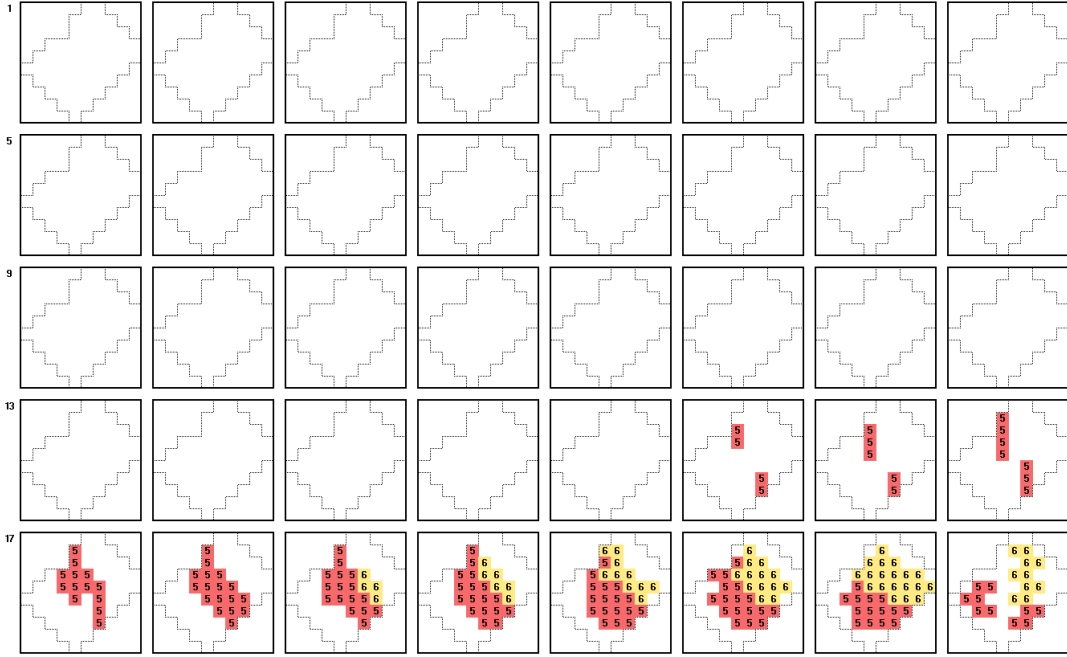


Figure 8: Partitioning of subcircuit 5 to minimize all-to-all communication for the 20-cycle, 53-qubit Sycamore circuit shown in Fig. 1.

5 Estimated running times

We estimate running times for the above simulation strategy on the Summit supercomputer using a combination of published performance figures and early IBM internal benchmarks.

Because we directly employ the partitioning strategy of [9] in a recursive fashion, and the resulting 45-qubit disk slices coincide with the 45-qubit circuits simulated in [9], we use the performance figures in [9] to estimate per-disk-slice computational costs. This implicitly assumes that we are directly using the implementation described in [9] for the computations. Since [9] employs 8,192 nodes of the Cori II supercomputer, we can more easily extrapolate predicted performance across a corresponding 8,192 sockets on Summit.

To account for the differences between the gate set of [9] and Sycamore circuits, we use the following two facts: in [9], gates are aggregated together into k -qubit kernels represented by $2^k \times 2^k$ unitary matrices; and amplitudes are updated using matrix-matrix and/or matrix-vector calculations. The gate aggregation effectively normalizes computations across gate sets, making them independent from the details of individual gates. For simulations performed on Cori II, gate aggregation in [9] uses $k_{max} = 5$, with actual kernel sizes sometimes being less than 5 qubits depending on the aggregated gates. To leverage the performance figures reported in [9], we therefore perform the same form of gate aggregation on Sycamore circuits. Tables 1 and 2 summarize the results obtained with these gate aggregations for the 53- and 54-qubit circuits illustrated in Figs. 1 and 2, respectively. In these tables, the “5-qubit kernels per disk slice” column identifies the number of aggregate gates constructed for the corresponding subcircuit or sub-subcircuit.

After gate aggregation, we estimate execution times for gate operations using Tables 1 and 2 in [9]. Specifically, we use the “Time” and “Comm.” columns of Table 2 in [9] to estimate computation time from total execution time, by factoring out the reported percentage of communication and synchronization time. We then divide the computation times by the number of aggregate gates (i.e., clusters) listed

Tensor	Disk transfers per disk slice	All-to-alls per disk slice	5Q kernels per disk slice	Tensor ranks per socket	Num gates	Contraction cost tot. FLOPs	Compute time (days)	% of total time	Achieved PFLOPS
1		0.000977	28	28	84	$1.181 \cdot 10^{21}$	0.002082	0.08%	0.0308
2		0.000977	25	27	84		0.001859	0.07%	0.0173
Contraction				31			0.117058	4.59%	116.7304
3.3			16	32	63		0.010658	0.42%	18.4865
3.4		1	6	32	23		0.003997	0.16%	17.9975
3.5		1	8	32	26		0.005329	0.21%	15.2587
Disk write	1	1							
Disk read	1	1							
4.4			11	32	49		0.007327	0.29%	20.9141
4.5		1	10	32	45		0.006661	0.26%	21.1275
Disk write	1	1							
Disk read	1	1							
5.5			9	32	35		0.005995	0.24%	18.2583
5.6		1	7	32	21		0.004663	0.18%	14.0850
Disk write	1	1							
Subtotals									
Compute			120			$1.181 \cdot 10^{21}$	0.165631	6.50%	87.4462
All-to-alls		9.001953					0.487725	19.13%	
Disk I/O	5						1.896296	74.37%	
Total	5	9.001953	120	32.67243	430		2.549652	100.00%	87.4462

Table 1: Running time estimates to simulate the 20-cycle, 53-qubit Sycamore circuit shown in Fig. 1. Tensors 3.3, 3.4, and 3.5 correspond to the partitionings of subcircuit 3 shown in Fig. 6, tensors 4.4 and 4.5 to the partitionings of subcircuit 4 shown in Fig. 7, and tensors 5.5 and 5.6 to the partitionings of subcircuit 5 shown in Fig. 8. The number of 5-qubit kernels is the number of aggregated gates spanning no more than 5 qubits, created by grouping gates together within each subcircuit. The contraction cost is the total number floating-point operations needed to perform the tensor contractions associated with entanglement indices, when tensors 1 and 2 are contracted in preparation for simulating subcircuit 3. The tensor ranks per socket indicate the sizes of the corresponding tensors in terms of the effective number of local qubits per socket. For entries above the subtotal line, the compute times are either the estimated times to perform gate operations based on the number of 5-qubit kernels, or the estimated time to perform the tensor 1 and 2 contractions, depending on the row in the table. Entries below the subtotal line factor in the costs of performing all-to-all communication and disk I/O. In the case of gate operations, the achieved PetaFLOPs per second column is the total number of floating-point operations without gate aggregation divided by the estimated compute time with gate aggregation.

Tensor	Disk transfers per disk slice	All-to-alls per disk slice	5Q kernels per disk slice	Tensor ranks per socket	Num gates	Contraction cost tot. FLOPs	Compute time (days)	% of total time	Achieved PFLOPS
1		0.001953	28	30	84	$9.445 \cdot 10^{21}$	0.004164	0.07%	0.0616
2		0.001953	26	30	87		0.003867	0.07%	0.0687
Contraction				33			0.936466	16.14%	116.7304
3.3			15	32	59		0.019984	0.42%	18.4865
3.4		1	8	32	31		0.010658	0.18%	18.1931
3.5		1	8	32	27		0.010658	0.18%	15.8456
Disk write	1	1							
Disk read	1	1							
4.4			11	32	49		0.014655	0.25%	20.9141
4.5		1	10	32	45		0.013323	0.23%	21.1275
Disk write	1	1							
Disk read	1	1							
5.5			9	32	37	0.011990	0.21%	19.3016	
5.6		1	7	32	21	0.009326	0.16%	14.0850	
Disk write	1	1							
Subtotals						$9.445 \cdot 10^{21}$			
Compute			122				1.035091	17.84%	107.2342
All-to-alls		9.003906					0.975661	16.81%	
Disk I/O	5						3.792593	65.35%	
Total	5	9.003906	122	33.80735	440		5.803345	100.00%	107.2342

Table 2: Running time estimates to simulate the 20-cycle, 54-qubit Sycamore circuit shown in Fig. 2. Tensors 3.3, 3.4, and 3.5 correspond to the partitionings of subcircuit 3 shown in Fig. 9, tensors 4.4 and 4.5 to the partitionings of subcircuit 4 shown in Fig. 10, and tensors 5.5 and 5.6 to the partitionings of subcircuit 5 shown in Fig. 11. The number of 5-qubit kernels is the number of aggregated gates spanning no more than 5 qubits, created by grouping gates together within each subcircuit. The contraction cost is the total number floating-point operations needed to perform the tensor contractions associated with entanglement indices, when tensors 1 and 2 are contracted in preparation for simulating subcircuit 3. The tensor ranks per socket indicate the sizes of the corresponding tensors in terms of the effective number of local qubits per socket. For entries above the subtotal line, the compute times are either the estimated times to perform gate operations based on the number of 5-qubit kernels, or the estimated time to perform the tensor 1 and 2 contractions, depending on the row in the table. Entries below the subtotal line factor in the costs of performing all-to-all communication and disk I/O. In the case of gate operations, the achieved PetaFLOPs per second column is the total number of floating-point operations without gate aggregation divided by the estimated compute time with gate aggregation.

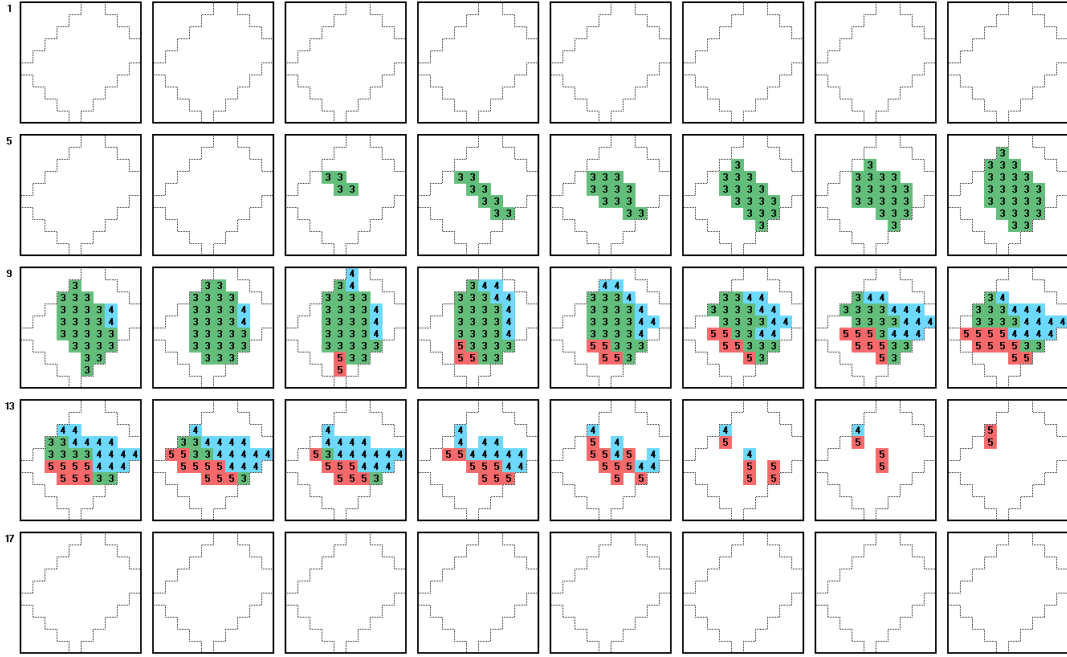


Figure 9: Partitioning of subcircuit 3 to minimize all-to-all communication for the 20-cycle, 54-qubit Sycamore circuit shown in Fig. 2.

in Table 1 in [9] to obtain overall average execution times per aggregate gate. These averages can be used to estimate execution times for arbitrary numbers of aggregate gates, assuming simulations are performed on Cori II. To obtain corresponding time estimates for Summit, we scale the estimates by the ratio of the High Performance Linpack (HPL) benchmark figure for Cori II (14,014.70 TeraFLOPs/sec) versus Summit (148,600.00 TeraFLOPs/sec); this accounts for the substantially greater performance of Summit when performing, e.g., the matrix-vector calculations entailed by the use of gate aggregation. The calculations for 45-qubit simulations yield an expected execution time of 2.38380 seconds per aggregate gate on Cori II, and 0.22482 seconds per aggregated gate on Summit. The runtime estimates shown in Tabs. 1 and 2 for tensors 3, 4 and 5 are obtained by multiplying the number of aggregate gates in each of their sub-subcircuits by 0.22482 seconds, and further multiplying by the number of disk slices per tensor (i.e., 256 slices for the 53-qubit circuit and 512 slices for the 54-qubit circuit). Tensors 1 and 2, on the other hand, represent 30-qubit calculations or less; therefore, we use the 30-qubit performance figures from Tables 1 and 2 in [9] to obtain an estimated 0.025097 seconds per aggregate gate on Summit for these tensors.

The “achieved FLOPs per second” columns in Tabs. 1 and 2 provide a sanity check for the above time estimates. For rows corresponding to gate operations, this column reports the number of floating-point operations that would be performed without gate aggregation divided by the estimated execution times. As such, the resulting figures provide an indication of the implied efficiency of the time estimates. As can be seen, the time estimates for gate operations yield results that are all near or below 11% of the 191 PetaFLOPs/sec peak double-precision performance expected across 8,192 sockets. Therefore, there is room to potentially improve upon these estimates by leveraging the capabilities of Summit’s NVIDIA GPUs: this would allow the simulation of individual gate operations, without resorting to gate aggregation, and the use of cuBLAS routines to implement the corresponding matrix-vector operations.

To obtain time estimates for the contractions of tensors 1 and 2, we use the performance figures reported in Table 1 in [17]. The simulation method presented in [16, 17] employs the “bristle-brush”

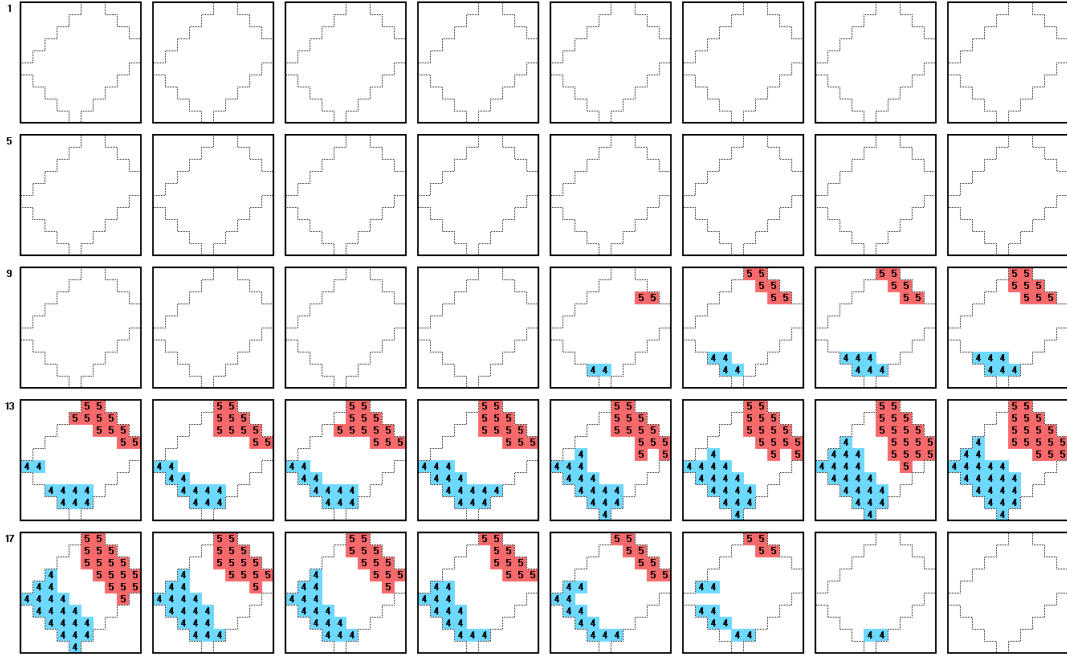


Figure 10: Partitioning of subcircuit 4 to minimize all-to-all communication for the 20-cycle, 54-qubit Sycamore circuit shown in Fig. 2.

strategy outlined in [13]. A key characteristic of this simulation strategy is that computations are dominated by very large tensor contractions across many tensor indices simultaneously. Consequently, we directly use the performance figures reported in Table 1 in [17] to estimate contraction times. Because we assume double-precision calculations, as in [9], we convert the performance figures in [17] from single-precision to double-precision. To do so, we multiply the single-precision computation rates of [17] by the ratio between the double-precision (7.8 TeraFLOPs/sec) and single-precision (15.7 TeraFLOPs/sec) peak performance rate of Summit’s NVIDIA GPUs. Performing this calculation and taking the worst case yields as estimated 14.249 TeraFLOPs per socket (116.73 PetaFLOPs/sec for 8,192 sockets). We use this rate in Tabs. 1 and 2 to estimate execution times for the contraction of tensors 1 and 2.

We estimate all-to-all and disk I/O times using results from early IBM internal benchmarks. These benchmarks indicate that a network injection rate of 7 GB/sec per node (3.5 GB/sec per socket) should be easily achieved during an all-to-all across the entire machine. This figure represents $\approx 30\%$ of the 23 GB/sec per node peak injection rate (11.5 GB/sec per socket) that characterizes the bisection bandwidth of Summit. The maximum reported file-system transfer rate is 2.2 TB/sec for random-access I/O (2.5 TB/sec for pure sequential I/O). We assume that all disk storage operations use single precision, while in-memory calculations use double precision. Thus, the estimates in Tabs. 1 and 2 are based on a transfer rate of 2 TB/sec and a storage density of 8 bytes per amplitude (i.e., single-precision complex). Benchmark tests suggest that allocating only a subset of nodes to the task of performing disk I/O can be more efficient because it may avoid contention; those nodes then become the distribution points to the rest of the system when spreading computations across a majority of the nodes. Tabs. 1 and 2 model this arrangement by incorporating an all-to-all communication cost for every disk read or write operation.

The resulting estimated running times are summarized in Tabs. 1 and 2. As these tables show, with the performance model discussed in this section we obtain an overall estimate of 2.55 days to compute all 2^{53} amplitudes of a 20-cycle, 53-qubit, Sycamore ABCDCDAB circuit with all amplitudes stored on disk, and 5.80 days for the corresponding 54-qubit circuit. To store amplitudes on disk in single

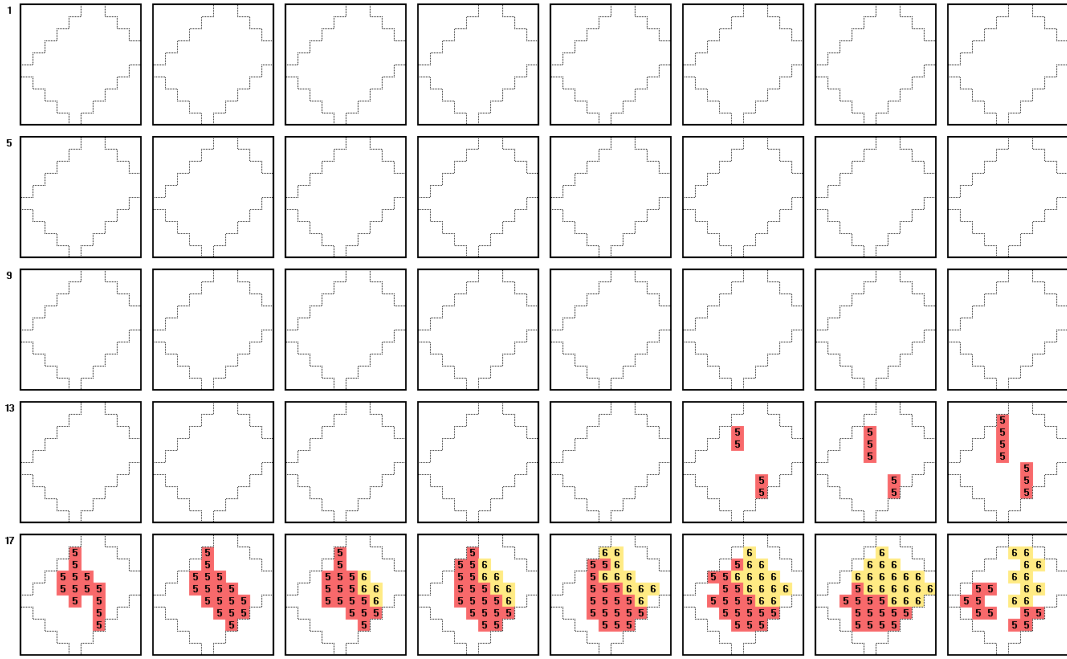


Figure 11: Partitioning of subcircuit 5 to minimize all-to-all communication for the 20-cycle, 54-qubit Sycamore circuit shown in Fig. 2.

precision, 64 PiB of disk space are required for 53-qubit circuits, and 128 PiB for 54-qubit circuits. Both fit within the 250 PiB available on Summit.

The above analysis can be repeated for all depths suggested by Figs. 3 and 4; i.e., 10, 14, 20, 24, 28, 32, and 36 cycles. Doing so yields the results reported in Tables 3 and 4, and plotted in Fig. 12. As these tables and figure illustrate, estimated execution times grow linearly with the depth of the circuits. We remark that the required disk space remains constant, because with the above approach there is a maximum number of slices that are stored on disk at any given time. Thus, the disk occupation is 64 PiB for 53-qubit circuits and 128 PiB for 54-qubit circuits, regardless of the number of cycles.

Number of Cycles	Disk Xfers per Disk Slice	All-to-Alls per Disk Slice	5-Qubit Kernels per Disk Slice	Run Time (days)
10	1	3.002	65	0.67
14	3	6.002	89	1.61
20	5	9.002	120	2.55
24	7	13.002	141	3.54
28	9	16.002	162	4.47
32	11	20.002	182	5.46
36	13	24.002	206	6.45

Table 3: Estimates of total run times for simulating 53-qubit, Sycamore ABCDCDAB circuits of various depths.

Number of Cycles	Disk Xfers per Disk Slice	All-to-Alls per Disk Slice	5-Qubit Kernels per Disk Slice	Run Time (days)
10	1	3.004	66	2.05
14	3	6.004	90	3.92
20	5	9.004	122	5.80
24	7	13.004	144	7.78
28	9	16.004	166	9.65
32	11	20.004	187	11.63
36	13	24.004	211	13.62

Table 4: Estimates of total run times for simulating 54-qubit, Sycamore ABCDCDAB circuits of various depths.

53- and 54-Qubit Sycamore Circuits with Single Precision Storage to Disk (8 bytes per amplitude)

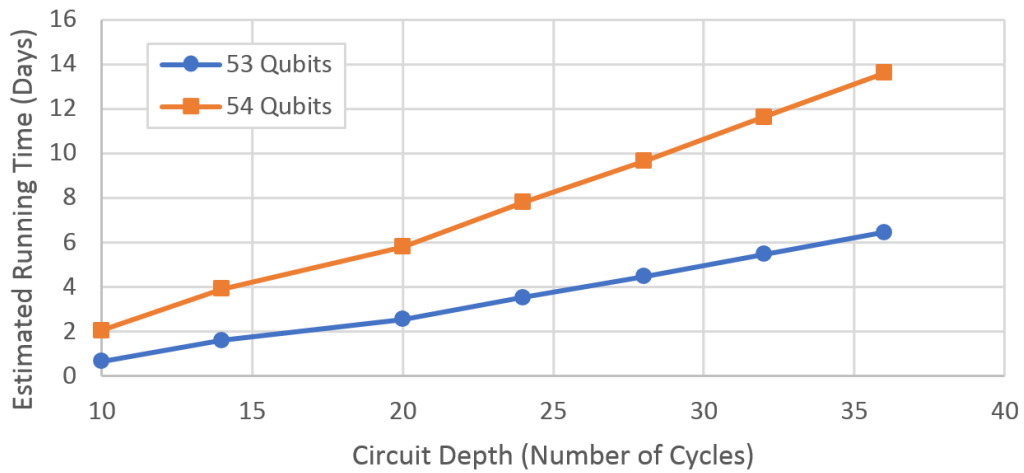


Figure 12: Graph of total runtime estimates for fully simulating both 53- and 54-qubit, Sycamore ABCDCDAB circuits of various depths, with all amplitudes calculated and stored on disk.

References

- [1] S. Aaronson and L. Chen. Complexity-theoretic foundations of quantum supremacy experiments. *arXiv preprint arXiv:1612.05903*, 2016.
- [2] S. Boixo, S. V. Isakov, V. N. Smelyanskiy, R. Babbush, N. Ding, Z. Jiang, M. J. Bremnen, J. M. Martinis, and H. Neven. Characterizing quantum supremacy in near-term devices. *Nature Physics*, 14(6):595–600, 2018.
- [3] S. Boixo, S. V. Isakov, V. N. Smelyanskiy, and H. Neven. Simulation of low-depth quantum circuits as complex undirected graphical models. *arXiv preprint arXiv:1712.05384*, 2017.
- [4] D. Castelvecchi. Quantum computers ready to leap out of the lab in 2017. *Nature*, 541:9–10, 2017.
- [5] J. Chen, F. Zhang, M. Chen, C. Huang, M. Newman, and Y. Shi. Classical simulation of intermediate-size quantum circuits. *arXiv preprint arXiv:1805.01450*, 2018.
- [6] M.-C. Chen, R. Li, L. Gan, X. Zhu, G. Yang, C.-Y. Lu, and J.-W. Pan. Quantum teleportation-inspired algorithm for sampling large random quantum circuits. *arXiv preprint arXiv:1901.05003*, 2019.
- [7] Z. Chen, Q. Zhou, C. Xue, X. Yang, G. Guo, and G. Guo. 64-qubit quantum circuit simulation. *arXiv preprint arXiv:1802.06952*, 2018.
- [8] C. Guo, Y. Liu, M. Xiong, S. Xue, X. Fu, A. Huang, X. Qiang, P. Xu, J. Liu, S. Zheng, H.-L. Huang, M. Deng, D. Poletti, W.-S. Bao, and J. Wu. General-purpose quantum circuit simulator with projected entangled-pair states and the quantum supremacy frontier. *arXiv preprint arXiv:1905.08394*, 2019.
- [9] T. Häner and D. S. Steiger. 0.5 petabyte simulation of a 45-qubit quantum circuit. In *Proceedings of the International Conference for High Performance Computing, Networking, Storage and Analysis, SC '17*, pages 33:1–33:10, New York, NY, USA, 2017. ACM.
- [10] R. Li, B. Wu, M. Ying, X. Sun, and G. Yang. Quantum supremacy circuit simulation on sunway taihulight. *arXiv preprint arXiv:1804.04797*, 2018.
- [11] I. L. Markov, A. Fatima, S. V. Isakov, and S. Boixo. Quantum supremacy is both closer and farther than it appears. *arXiv preprint arXiv:1807.10749*, 2018.
- [12] I. L. Markov and Y. Shi. Simulating quantum computation by contracting tensor networks. *SIAM Journal on Computing*, 38(3):963–981, 2008.
- [13] E. Pednault. Quantum computing—breaking through the 49 qubit simulation barrier. *IBM Research Blog posting also posted on phys.org* (<https://www.ibm.com/blogs/research/2017/10/quantum-computing-barrier/> and <https://phys.org/news/2017-10-quantum-computing-breaking-qubit-simulation-barrier.html>), 2017.
- [14] E. Pednault, J. A. Gunnels, G. Nannicini, L. Horesh, T. Magerlein, E. Solomonik, and R. Wisnieff. Breaking the 49-qubit barrier in the simulation of quantum circuits. *arXiv preprint arXiv:1710.05867*, 2017.
- [15] E. G. Rieffel and al. Quantum supremacy using a programmable superconducting processor. *NASA AMES Research Center Technical Report NASA/TP-2019-220319*, 2019.

- [16] B. Villalonga, S. Boixo, B. Nelson, C. Henze, E. Rieffel, R. Biswas, and S. Mandrà. A flexible high-performance simulator for the verification and benchmarking of quantum circuits implemented on real hardware. *arXiv preprint arXiv:1811.09599*, 2018.
- [17] B. Villalonga, D. Lyakh, S. Boixo, H. Neven, T. S. Humble, R. Biswas, E. G. Rieffel, A. Ho, and S. Mandrà. Establishing the quantum supremacy frontier with a 281 pflop/s simulation. *arXiv preprint arXiv:1905.00444*, 2019.
- [18] F. Zhang, C. Huang, M. Newman, J. Cai, H. Yu, Z. Tian, B. Yuan, H. Xu, J. Wu, X. Gao, J. Chen, M. Szegedy, and Y. Shi. Alibaba cloud quantum development kit: Large-scale classical simulation of quantum circuits. *arXiv preprint arXiv:1907.11217*, 2019.

A Implementation details

We give a full description of the implementation of the tensor computations, including cache blocking to create the 5-qubit aggregate gates. Further optimizations might be possible; this description is meant as a viable proof of concept modeled on [9].

We describe how to interpret each line in the listing. Qubits are numbered from 0 to $n - 1$. The “Mode” column indicates the type of information contained in the corresponding line. We give an overview of each of the eight possible modes.

- “define”: the first define line indicates the total number of qubits, the second define line describes the qubit indices used to address logical files on disk.
- “new”:
 - if the “Gate” column contains “tensor”, it describes a new tensor. The column “Arguments” indicates the corresponding number of local qubits and of global qubits, followed by the indices of the qubits in the tensor, starting with local qubits and ending with global qubits.
 - if the “Gate” column contains “cache”, it indicates how to partition gates into 5-qubit aggregate gates.
- “gate”: describes a gate. All gates are two-qubit gates after circuit transformations, as discussed in the paper; the “Arguments” column indicates the qubits involved.
- “entgl”: describes the introduction of an entanglement index due to a deferred contraction between tensors.
 - if the “Gate” column contains “tensor”, it describes the new tensor with the corresponding list of entanglement indices (labeled with negative numbers).
 - if the “Gate” column contains “EI” or “E2Q”, it describes synthesized gate operations that are employed when introducing entanglement indices.
- “slice”: lists the indices of the qubits that are sliced on the first level of the recursive scheme.
- “all2all”: indicates a communication between nodes used to rearrange tensor indices in preparation for a contraction, or to swap which qubits are local and which ones are global.
- “write”: indicates which qubit indices to fix, in order to write a slice to disk.
- “read”: indicates which qubit indices to fix, in order to read a slice from disk.

Note that in the listings, gate $2Q$ together with the level of the gate in the circuit and the qubits to which that gate is applied refers to a specific instance of one of the gates shown in Figs. 1 and 2 with its own potentially unique associated unitary matrix.

To define the synthesized gate operations EI and $E2Q$, suppose one of these $2Q$ gate bridges qubits a and b in Tensors 1 and 2, respectively. Let ϕ_a and χ_b be the corresponding tensors prior to applying that $2Q$ gate. Then the resulting quantum state is given by

$$\psi_{a'',b''} = \sum_{a,b} 2Q_{a'',b'',a,b} \cdot \phi_a \cdot \chi_b = \sum_{a',a,b} I_{a'',a'} \cdot 2Q_{a',b'',a,b} \cdot \phi_a \cdot \chi_b \quad (2)$$

where I is the identity matrix. The above equation can be rewritten as

$$\psi_{a'',b''} = \sum_{a',a} \phi'_{a'',a',a} \cdot \chi'_{b'',a',a} \quad (3)$$

where

$$\phi'_{a'',a',a} = I_{a'',a'} \cdot \phi_a, \quad \chi'_{b'',a',a} = \sum_b 2Q_{a',b'',a,b} \cdot \chi_b \quad (4)$$

These last two equations define the *EI* and *E2Q* synthesized gate operations, respectively, where a'' is effectively the new index for qubit a , b'' the new index for qubit b , and a' and a are entanglement indices introduced through these synthesized gate operations. The equation above it defines the contraction performed to eliminate entanglement indices.

The following listing is for the 53-qubit circuit.

Tensor	Phase	Mode	Depth	Gate	Arguments
0	0	define	0	qubits	53
0	0	define	0	disk	0,1,2,3,4,5,6,7,8,23,24,25,26,27,28,29,30,49,50,51,52
1	1	new	0	tensor	27,0,0,1,2,3,4,5,6,7,8,9,10,11,12,13,14,15,16,17,18,19,20,21,22,23,24,25,26
1	1	new	0	cache	10,14,18,19,23
1	1	gate	1	2Q	14,10
1	1	gate	1	2Q	23,19
1	1	gate	3	2Q	18,14
1	1	gate	6	2Q	23,18
1	1	new	0	cache	2,6,10,18,23
1	1	gate	2	2Q	6,2
1	1	gate	4	2Q	10,6
1	1	new	0	cache	1,5,6,18,23
1	1	gate	2	2Q	5,1
1	1	gate	6	2Q	6,1
1	1	new	0	cache	5,9,14,18,23
1	1	gate	3	2Q	9,5
1	1	gate	6	2Q	14,9
1	1	new	0	cache	0,5,18,23
1	1	gate	5	2Q	5,0
1	1	new	0	cache	18,22,23,26
1	1	gate	2	2Q	26,22
1	1	new	0	cache	18,20,23,24,26
1	1	gate	1	2Q	24,20
1	1	new	0	cache	12,16,18,20,23
1	1	gate	2	2Q	16,12
1	1	gate	4	2Q	20,16
1	1	new	0	cache	18,20,21,23,25
1	1	gate	2	2Q	25,21
1	2	entgl	0	tensor	27,8,0,1,2,3,4,5,6,7,8,9,10,11,12,13,14,15,16,17,18,19,20,21,22,23,24,25,26,-1,-2,-3,-4,-5,-6,-7,-8,-9,-10,-11,-12,-13,-14
1	2	entgl	3	EI	25,-1,-2
1	2	entgl	3	EI	24,-3,-4
1	2	entgl	4	EI	26,-5,-6
1	2	entgl	7	EI	23,-9,-10
1	2	new	0	cache	18,20,23,25
1	2	gate	5	2Q	25,20
1	2	gate	10	2Q	23,18
1	2	new	0	cache	11,14,15,19,24
1	2	gate	2	2Q	15,11
1	2	gate	3	2Q	19,15
1	2	gate	5	2Q	24,19
1	2	gate	8	2Q	19,14
1	2	new	0	cache	9,14,19,24,25
1	2	gate	10	2Q	14,9
1	3	entgl	0	tensor	27,12,0,1,2,3,4,5,6,7,8,9,10,11,12,13,14,15,16,17,18,19,20,21,22,23,24,25,26,-1,-2,-3,-4,-5,-6,-7,-8,-9,-10,-11,-12,-13,-14
1	3	entgl	7	EI	24,-7,-8
1	3	entgl	8	EI	25,-13,-14
1	3	new	0	cache	10,14,15,19,24
1	3	gate	6	2Q	15,10

Tensor	Phase	Mode	Depth	Gate	Arguments
1	3	gate	9	2Q	24,19
1	3	gate	12	2Q	19,14
1	3	new	0	cache	0,5,10,15,20
1	3	gate	7	2Q	20,15
1	3	gate	8	2Q	10,5
1	3	gate	9	2Q	5,0
1	3	gate	10	2Q	15,10
1	3	gate	12	2Q	10,5
1	3	new	0	cache	10,14,18,20,25
1	3	gate	9	2Q	25,20
1	3	gate	13	2Q	14,10
1	3	gate	15	2Q	18,14
1	3	new	0	cache	13,15,17,20,21
1	3	gate	1	2Q	17,13
1	3	gate	4	2Q	21,17
1	3	gate	11	2Q	20,15
1	3	new	0	cache	3,7,11,21,26
1	3	gate	1	2Q	7,3
1	3	gate	4	2Q	11,7
1	3	gate	6	2Q	26,21
1	3	new	0	cache	1,5,6,11,16
1	3	gate	5	2Q	16,11
1	3	gate	8	2Q	11,6
1	3	gate	10	2Q	6,1
1	3	gate	14	2Q	5,1
1	3	new	0	cache	0,1,5,9,26
1	3	gate	15	2Q	9,5
1	3	gate	18	2Q	5,1
1	3	gate	19	2Q	9,5
1	3	gate	21	2Q	5,0
1	3	new	0	cache	6,11,15,16,21
1	3	gate	7	2Q	21,16
1	3	gate	9	2Q	16,11
1	3	gate	12	2Q	11,6
1	3	gate	14	2Q	15,11
1	3	new	0	cache	3,4,8,12,13
1	3	gate	1	2Q	8,4
1	3	gate	3	2Q	12,8
1	3	gate	5	2Q	8,3
1	3	gate	7	2Q	13,8
1	3	gate	9	2Q	8,3
1	3	gate	11	2Q	13,8
1	3	gate	13	2Q	8,4
1	3	new	0	cache	2,6,7,12,17
1	3	gate	5	2Q	17,12
1	3	gate	6	2Q	7,2
1	3	gate	7	2Q	12,7
1	3	gate	10	2Q	7,2
1	3	gate	14	2Q	6,2
1	3	new	0	cache	6,9,10,14,18
1	3	gate	16	2Q	10,6
1	3	gate	17	2Q	14,10
1	3	gate	19	2Q	18,14
1	3	gate	22	2Q	14,9
1	3	new	0	cache	1,2,6,10,26
1	3	gate	18	2Q	6,2
1	3	gate	20	2Q	10,6
1	3	gate	22	2Q	6,1
1	3	new	0	cache	7,12,13,17,22
1	3	gate	8	2Q	22,17
1	3	gate	9	2Q	17,12
1	3	gate	11	2Q	12,7
1	3	gate	12	2Q	22,17
1	3	gate	13	2Q	17,13
1	3	new	0	cache	3,7,11,21,26
1	3	gate	13	2Q	7,3
1	3	gate	16	2Q	11,7
1	3	gate	17	2Q	7,3

Tensor	Phase	Mode	Depth	Gate	Arguments
1	4	entgl	0	tensor	28,13,0,1,2,3,4,5,6,7,8,9,10,11,12 ,13,14,15,16,17,18,19,20,21,22,23,24,25,26,-1 ,-2,-3,-4,-5,-6,-7,-8,-9,-10,-11,-12,-13,-14
1	4	entgl	8	EI	26,-11,-12
1	4	new	0	cache	8,12,16,21,26
1	4	gate	10	2Q	26,21
1	4	gate	11	2Q	21,16
1	4	gate	14	2Q	16,12
1	4	gate	15	2Q	12,8
1	4	new	0	cache	4,8
1	4	gate	17	2Q	8,4
2	5	new	0	tensor	26,0,27,28,29,30,31,32,33,34,35,36,37,38,39 ,40,41,42,43,44,45,46,47,48,49,50,51,52
2	5	new	0	cache	36,40,44,45,49
2	5	gate	1	2Q	49,45
2	5	gate	2	2Q	40,36
2	5	gate	3	2Q	44,40
2	5	gate	6	2Q	49,44
2	5	gate	10	2Q	49,44
2	5	new	0	cache	30,34,37,41,45
2	5	gate	2	2Q	34,30
2	5	gate	2	2Q	41,37
2	5	gate	4	2Q	45,41
2	5	new	0	cache	29,33,34,38,42
2	5	gate	1	2Q	33,29
2	5	gate	1	2Q	42,38
2	5	gate	3	2Q	38,34
2	5	new	0	cache	29,30,34,39,43
2	5	gate	1	2Q	43,39
2	6	entgl	0	tensor	26,4,27,28,29,30,31,32,33,34,35,36,37,38,39 ,40,41,42,43,44,45,46,47,48,49,50,51,52,-1,-2 ,-3,-4,-5,-6,-7,-8,-9,-10,-11,-12,-13,-14
2	6	entgl	4	E2Q	29,-5,-6
2	6	entgl	8	E2Q	30,-11,-12
2	6	new	0	cache	29,33,34,37,39
2	6	gate	3	2Q	37,33
2	6	gate	6	2Q	34,29
2	6	gate	7	2Q	39,34
2	6	new	0	cache	27,29,31,34,39
2	6	gate	2	2Q	31,27
2	6	new	0	cache	29,31,34,35,39
2	6	gate	4	2Q	35,31
2	6	new	0	cache	35,40,45,46,50
2	6	gate	2	2Q	50,46
2	6	gate	5	2Q	40,35
2	6	gate	6	2Q	50,45
2	6	gate	8	2Q	45,40
2	6	gate	9	2Q	40,35
2	6	gate	10	2Q	50,45
2	6	gate	12	2Q	45,40
2	6	new	0	cache	29,34,39,45,49
2	6	gate	13	2Q	49,45
2	6	new	0	cache	29,34,39,42,46
2	6	gate	4	2Q	46,42
2	6	new	0	cache	29,34,37,39,42
2	6	gate	6	2Q	42,37
2	7	entgl	0	tensor	26,8,27,28,29,30,31,32,33,34,35,36,37,38,39 ,40,41,42,43,44,45,46,47,48,49,50,51,52,-1,-2 ,-3,-4,-5,-6,-7,-8,-9,-10,-11,-12,-13,-14
2	7	entgl	3	E2Q	27,-3,-4
2	7	entgl	8	E2Q	29,-13,-14
2	7	new	0	cache	28,29,32,34,39
2	7	gate	1	2Q	32,28
2	7	gate	10	2Q	34,29
2	7	gate	11	2Q	39,34
2	7	new	0	cache	27,32,36,37,41
2	7	gate	4	2Q	36,32
2	7	gate	5	2Q	32,27

Tensor	Phase	Mode	Depth	Gate	Arguments
2	7	gate	6	2Q	41,36
2	7	gate	8	2Q	37,32
2	7	new	0	cache	27,41,46,47,51
2	7	gate	2	2Q	51,47
2	7	gate	5	2Q	51,46
2	7	gate	8	2Q	46,41
2	7	gate	9	2Q	51,46
2	7	new	0	cache	31,36,40,41,44
2	7	gate	7	2Q	36,31
2	7	gate	10	2Q	41,36
2	7	gate	11	2Q	36,31
2	7	gate	14	2Q	40,36
2	7	gate	15	2Q	44,40
2	7	new	0	cache	27,32,41,46,50
2	7	gate	12	2Q	46,41
2	7	gate	14	2Q	50,46
2	7	new	0	cache	28,33,38,43,47
2	7	gate	3	2Q	47,43
2	7	gate	5	2Q	43,38
2	7	new	0	cache	37,42,47,48,52
2	7	gate	1	2Q	52,48
2	7	gate	5	2Q	52,47
2	7	gate	7	2Q	47,42
2	7	gate	9	2Q	52,47
2	7	gate	10	2Q	42,37
2	7	gate	11	2Q	47,42
2	8	entgl	0	tensor	26,12,27,28,29,30,31,32,33,34,35,36,37,38,39 ,40,41,42,43,44,45,46,47,48,49,50,51,52,-1,-2 , -3,-4,-5,-6,-7,-8,-9,-10,-11,-12,-13,-14
2	8	entgl	3	E2Q	28,-1,-2
2	8	entgl	7	E2Q	27,-9,-10
2	8	new	0	cache	27,32,37,41,45
2	8	gate	9	2Q	32,27
2	8	gate	12	2Q	37,32
2	8	gate	14	2Q	41,37
2	8	gate	16	2Q	45,41
2	8	new	0	cache	45,47,49,51
2	8	gate	14	2Q	51,47
2	8	gate	17	2Q	49,45
2	8	new	0	cache	28,33,38,43,48
2	8	gate	6	2Q	33,28
2	8	gate	7	2Q	48,43
2	8	gate	8	2Q	38,33
2	8	gate	9	2Q	43,38
2	8	gate	11	2Q	48,43
2	8	new	0	cache	28,39,43,47,51
2	8	gate	13	2Q	43,39
2	8	gate	15	2Q	47,43
2	8	gate	17	2Q	43,39
2	8	gate	18	2Q	51,47
2	8	gate	19	2Q	47,43
2	8	new	0	cache	28,33,47,48,52
2	8	gate	13	2Q	52,48
2	8	gate	17	2Q	52,48
2	8	gate	21	2Q	52,47
2	9	entgl	0	tensor	27,13,27,28,29,30,31,32,33,34,35,36,37,38,39 ,40,41,42,43,44,45,46,47,48,49,50,51,52,-1,-2 , -3,-4,-5,-6,-7,-8,-9,-10,-11,-12,-13,-14
2	9	entgl	7	E2Q	28,-7,-8
2	9	new	0	cache	28,33,38,42,46
2	9	gate	10	2Q	33,28
2	9	gate	12	2Q	38,33
2	9	gate	13	2Q	42,38
2	9	gate	16	2Q	46,42
2	9	new	0	cache	46,50
2	9	gate	18	2Q	50,46
0	10	slice	0	disk	0,1,2,3,49,50,51,52
1	10	all2all	0	tensor	30,7,-1,-2,-3,-4,-5,-6,-7,-8,-9,-10,-11,-12,-13

Tensor	Phase	Mode	Depth	Gate	Arguments
2	10	all2all	0	tensor	,-14,11,12,13,14,15,16,17,18,19,20,21,22,23,24 ,25,26,4,5,6,7,8,9,10 30,6,-1,-2,-3,-4,-5,-6,-7,-8,-9,-10,-11,-12,-13 ,-14,27,28,29,30,31,32,33,34,35,36,37,38,39,40 ,41,42,43,44,45,46,47,48
3	1	new	0	tensor	32,13,11,12,13,14,15,16,17,18,19,20,21,22,23 ,24,25,26,27,28,29,30,31,32,33,34,35,36,37,38 ,39,40,41,42,4,5,6,7,8,9,10,43,44,45,46 ,47,48
3	1	new	0	cache	15,18,19,23,27
3	1	gate	11	2Q	27,23
3	1	gate	13	2Q	23,19
3	1	gate	15	2Q	19,15
3	1	gate	17	2Q	23,19
3	1	gate	22	2Q	23,18
3	1	new	0	cache	26,30,34,38,42
3	1	gate	12	2Q	30,26
3	1	gate	14	2Q	34,30
3	1	gate	15	2Q	38,34
3	1	gate	17	2Q	42,38
3	1	gate	18	2Q	34,30
3	1	gate	19	2Q	38,34
3	1	new	0	cache	11,15,19,27,31
3	1	gate	14	2Q	31,27
3	1	gate	18	2Q	15,11
3	1	gate	19	2Q	19,15
3	1	new	0	cache	24,28,32,36,40
3	1	gate	11	2Q	28,24
3	1	gate	13	2Q	32,28
3	1	gate	16	2Q	36,32
3	1	gate	18	2Q	40,36
3	1	new	0	cache	20,24,27,31,35
3	1	gate	13	2Q	24,20
3	1	gate	15	2Q	27,24
3	1	gate	16	2Q	35,31
3	1	gate	18	2Q	31,27
3	1	gate	20	2Q	35,31
3	1	new	0	cache	16,19,20,24,27
3	1	gate	16	2Q	20,16
3	1	gate	17	2Q	24,20
3	1	gate	19	2Q	27,24
3	1	gate	21	2Q	24,19
3	1	new	0	cache	12,14,16,19,20
3	1	gate	18	2Q	16,12
3	1	gate	20	2Q	20,16
3	1	gate	24	2Q	19,14
3	1	new	0	cache	25,29,33,37,41
3	1	gate	12	2Q	29,25
3	1	gate	13	2Q	33,29
3	1	gate	15	2Q	37,33
3	1	gate	18	2Q	41,37
3	1	new	0	cache	22,26,29,33,34
3	1	gate	14	2Q	26,22
3	1	gate	16	2Q	29,26
3	1	gate	17	2Q	33,29
3	1	gate	18	2Q	26,22
3	1	gate	20	2Q	29,26
3	1	gate	22	2Q	34,29
3	1	new	0	cache	33,34,37,39
3	1	gate	19	2Q	37,33
3	1	gate	23	2Q	39,34
3	1	new	0	cache	21,25,28,32,36
3	1	gate	14	2Q	25,21
3	1	gate	15	2Q	28,25
3	1	gate	17	2Q	32,28
3	1	gate	20	2Q	36,32
3	1	new	0	cache	18,23,27,32
3	1	gate	21	2Q	32,27

Tensor	Phase	Mode	Depth	Gate	Arguments
3	1	gate	23	2Q	27,23
3	1	gate	26	2Q	23,18
3	1	new	0	cache	17,21,25,28,33
3	1	gate	16	2Q	21,17
3	1	gate	18	2Q	25,21
3	1	gate	19	2Q	28,25
3	1	gate	22	2Q	33,28
3	1	new	0	cache	20,25,29,34,39
3	1	gate	21	2Q	25,20
3	1	gate	24	2Q	29,25
3	1	gate	26	2Q	34,29
3	1	gate	27	2Q	39,34
3	1	new	0	cache	13,17,19,24,28
3	1	gate	17	2Q	17,13
3	1	gate	23	2Q	28,24
3	1	gate	25	2Q	24,19
3	1	new	0	cache	17,21,26,30
3	1	gate	20	2Q	21,17
3	1	gate	22	2Q	26,21
3	1	gate	24	2Q	30,26
3	2	all2all	0	tensor	32,13,17,18,19,20,21,22,23,24,25,26,27,28,29 ,30,31,32,33,34,35,36,37,38,39,40,41,42,43,44 ,45,46,47,48,4,5,6,7,8,9,10,11,12,13,14 ,15,16
3	2	new	0	cache	33,38,39,43,48
3	2	gate	21	2Q	43,38
3	2	gate	23	2Q	48,43
3	2	gate	24	2Q	38,33
3	2	gate	25	2Q	43,38
3	2	gate	27	2Q	48,43
3	2	gate	29	2Q	43,39
3	2	new	0	cache	24,28,33,38
3	2	gate	26	2Q	33,28
3	2	gate	27	2Q	28,24
3	2	gate	28	2Q	38,33
3	2	new	0	cache	32,37,42,46,47
3	2	gate	20	2Q	46,42
3	2	gate	22	2Q	42,37
3	2	gate	23	2Q	47,42
3	2	gate	24	2Q	37,32
3	2	gate	26	2Q	42,37
3	2	new	0	cache	23,27,28,32,37
3	2	gate	25	2Q	32,27
3	2	gate	27	2Q	27,23
3	2	gate	28	2Q	37,32
3	2	gate	29	2Q	32,28
3	2	new	0	cache	31,36,41,45
3	2	gate	20	2Q	45,41
3	2	gate	22	2Q	41,36
3	2	gate	23	2Q	36,31
3	2	new	0	cache	35,40,44
3	2	gate	19	2Q	44,40
3	2	gate	21	2Q	40,35
3	3	all2all	0	tensor	32,13,4,5,6,7,8,9,10,11,12,13,14,15,16 ,17,18,19,20,21,22,23,24,25,26,27,28,29,30,31 ,32,33,34,35,36,37,38,39,40,41,42,43,44,45,46 ,47,48
3	3	new	0	cache	9,14,19,23
3	3	gate	26	2Q	14,9
3	3	gate	28	2Q	19,14
3	3	gate	29	2Q	23,19
3	3	new	0	cache	10,15,20,25,29
3	3	gate	22	2Q	15,10
3	3	gate	23	2Q	20,15
3	3	gate	25	2Q	25,20
3	3	gate	28	2Q	29,25
3	3	new	0	cache	5,10,15,29,33
3	3	gate	24	2Q	10,5

Tensor	Phase	Mode	Depth	Gate	Arguments
3	3	gate	26	2Q	15,10
3	3	gate	29	2Q	33,29
3	3	new	0	cache	7,11,15,20,24
3	3	gate	20	2Q	11,7
3	3	gate	27	2Q	20,15
3	3	gate	29	2Q	24,20
3	3	new	0	cache	11,16,21,26,30
3	3	gate	21	2Q	16,11
3	3	gate	23	2Q	21,16
3	3	gate	26	2Q	26,21
3	3	gate	28	2Q	30,26
3	3	new	0	cache	6,11,16,30,34
3	3	gate	24	2Q	11,6
3	3	gate	25	2Q	16,11
3	3	gate	30	2Q	34,30
3	3	new	0	cache	16,21,25,28
3	3	gate	27	2Q	21,16
3	3	gate	30	2Q	25,21
3	3	gate	31	2Q	28,25
3	3	new	0	cache	8,12,17,22
3	3	gate	19	2Q	12,8
3	3	gate	21	2Q	17,12
3	3	gate	24	2Q	22,17
3	3	write	0	disk	0,1,2,3,49,50,51,52
4	1	read	0	disk	23,24,25,26,27,28,29,30
4	1	new	0	tensor	32,13,0,1,2,3,4,5,6,7,8,9,10,11,12 ,13,14,15,16,17,18,19,20,21,22,31,32,33,34,35 ,36,37,38,39,40,41,42,43,44,45,46,47,48,49,50 ,51,52
4	1	new	0	cache	0,5,10,14,18
4	1	gate	25	2Q	5,0
4	1	gate	28	2Q	10,5
4	1	gate	29	2Q	14,10
4	1	gate	31	2Q	18,14
4	1	new	0	cache	0,1,5,6,9
4	1	gate	26	2Q	6,1
4	1	gate	30	2Q	5,1
4	1	gate	31	2Q	9,5
4	1	gate	34	2Q	5,1
4	1	gate	35	2Q	9,5
4	1	gate	37	2Q	5,0
4	1	new	0	cache	6,11,15,19
4	1	gate	28	2Q	11,6
4	1	gate	30	2Q	15,11
4	1	gate	31	2Q	19,15
4	1	new	0	cache	2,6,7,10,12
4	1	gate	22	2Q	7,2
4	1	gate	23	2Q	12,7
4	1	gate	26	2Q	7,2
4	1	gate	30	2Q	6,2
4	1	gate	32	2Q	10,6
4	1	gate	34	2Q	6,2
4	1	new	0	cache	6,9,10,14,18
4	1	gate	33	2Q	14,10
4	1	gate	35	2Q	18,14
4	1	gate	36	2Q	10,6
4	1	gate	38	2Q	14,9
4	1	new	0	cache	1,6,12,17,22
4	1	gate	25	2Q	17,12
4	1	gate	28	2Q	22,17
4	1	gate	38	2Q	6,1
4	1	new	0	cache	3,8,13,17,21
4	1	gate	21	2Q	8,3
4	1	gate	23	2Q	13,8
4	1	gate	25	2Q	8,3
4	1	gate	27	2Q	13,8
4	1	gate	29	2Q	17,13
4	1	gate	32	2Q	21,17

Tensor	Phase	Mode	Depth	Gate	Arguments
4	1	gate	33	2Q	17,13
4	1	new	0	cache	3,7,11,12,15
4	1	gate	27	2Q	12,7
4	1	gate	29	2Q	7,3
4	1	gate	32	2Q	11,7
4	1	gate	33	2Q	7,3
4	1	gate	34	2Q	15,11
4	1	gate	36	2Q	11,7
4	1	new	0	cache	2,7,12,16,20
4	1	gate	30	2Q	16,12
4	1	gate	32	2Q	20,16
4	1	gate	38	2Q	7,2
4	1	new	0	cache	3,4,8,12,16
4	1	gate	29	2Q	8,4
4	1	gate	31	2Q	12,8
4	1	gate	33	2Q	8,4
4	1	gate	34	2Q	16,12
4	1	gate	35	2Q	12,8
4	1	gate	37	2Q	8,3
4	1	new	0	cache	8,13
4	1	gate	39	2Q	13,8
4	2	all2all	0	tensor	32,13,13,14,15,16,17,18,19,20,21,22,31,32,33 ,34,35,36,37,38,39,40,41,42,43,44,45,46,47,48 ,49,50,51,52,0,1,2,3,4,5,6,7,8,9,10 ,11,12
4	2	new	0	cache	38,42,47,48,52
4	2	gate	25	2Q	52,47
4	2	gate	27	2Q	47,42
4	2	gate	29	2Q	42,38
4	2	gate	29	2Q	52,48
4	2	gate	33	2Q	52,48
4	2	new	0	cache	41,43,46,47,51
4	2	gate	21	2Q	51,46
4	2	gate	24	2Q	46,41
4	2	gate	25	2Q	51,46
4	2	gate	30	2Q	51,47
4	2	gate	31	2Q	47,43
4	2	gate	34	2Q	51,47
4	2	new	0	cache	39,43,47,52
4	2	gate	33	2Q	43,39
4	2	gate	35	2Q	47,43
4	2	gate	37	2Q	52,47
4	2	new	0	cache	33,36,37,41,46
4	2	gate	26	2Q	41,36
4	2	gate	28	2Q	46,41
4	2	gate	30	2Q	41,37
4	2	gate	31	2Q	37,33
4	2	new	0	cache	40,42,45,46,50
4	2	gate	22	2Q	50,45
4	2	gate	24	2Q	45,40
4	2	gate	26	2Q	50,45
4	2	gate	30	2Q	50,46
4	2	gate	32	2Q	46,42
4	2	gate	34	2Q	50,46
4	2	new	0	cache	34,38,42,46,51
4	2	gate	31	2Q	38,34
4	2	gate	33	2Q	42,38
4	2	gate	36	2Q	46,42
4	2	gate	37	2Q	51,46
4	2	new	0	cache	31,35,36,40,45
4	2	gate	25	2Q	40,35
4	2	gate	27	2Q	36,31
4	2	gate	28	2Q	45,40
4	2	gate	30	2Q	40,36
4	2	new	0	cache	37,41,44,45,49
4	2	gate	22	2Q	49,44
4	2	gate	26	2Q	49,44
4	2	gate	29	2Q	49,45

Tensor	Phase	Mode	Depth	Gate	Arguments
4	2	gate	32	2Q	45,41
4	2	gate	33	2Q	49,45
4	2	gate	34	2Q	41,37
4	2	gate	36	2Q	45,41
4	2	new	0	cache	32,36,40,44,49
4	2	gate	31	2Q	44,40
4	2	gate	32	2Q	36,32
4	2	gate	34	2Q	40,36
4	2	gate	35	2Q	44,40
4	2	gate	38	2Q	49,44
4	2	new	0	cache	45,50
4	2	gate	38	2Q	50,45
4	2	write	0	disk	23,24,25,26,27,28,29,30
5	1	read	0	disk	0,1,2,3,49,50,51,52
5	1	new	0	tensor	32,13,4,5,6,7,8,9,10,11,12,13,14,15,16 ,17,18,19,20,21,22,23,24,25,26,27,28,29,30,31 ,32,33,34,35,36,37,38,39,40,41,42,43,44,45,46 ,47,48
5	1	new	0	cache	5,10,15,19,23
5	1	gate	33	2Q	23,19
5	1	gate	35	2Q	19,15
5	1	gate	38	2Q	15,10
5	1	gate	40	2Q	10,5
5	1	new	0	cache	7,12,17,21,25
5	1	gate	34	2Q	25,21
5	1	gate	36	2Q	21,17
5	1	gate	37	2Q	17,12
5	1	gate	39	2Q	12,7
5	1	new	0	cache	17,22,26,29,33
5	1	gate	30	2Q	26,22
5	1	gate	32	2Q	29,26
5	1	gate	33	2Q	33,29
5	1	gate	34	2Q	26,22
5	1	gate	36	2Q	29,26
5	1	gate	40	2Q	22,17
5	1	new	0	cache	21,26,30,34
5	1	gate	34	2Q	34,30
5	1	gate	38	2Q	26,21
5	1	gate	40	2Q	30,26
5	1	new	0	cache	18,23,25,28,32
5	1	gate	33	2Q	32,28
5	1	gate	35	2Q	28,25
5	1	gate	38	2Q	23,18
5	1	new	0	cache	20,24,27,31,35
5	1	gate	30	2Q	31,27
5	1	gate	31	2Q	27,24
5	1	gate	32	2Q	35,31
5	1	gate	33	2Q	24,20
5	1	gate	34	2Q	31,27
5	1	gate	35	2Q	27,24
5	1	gate	36	2Q	35,31
5	1	new	0	cache	14,16,19,20,24
5	1	gate	36	2Q	20,16
5	1	gate	37	2Q	24,19
5	1	gate	40	2Q	19,14
5	1	new	0	cache	6,11,16,21
5	1	gate	37	2Q	16,11
5	1	gate	39	2Q	21,16
5	1	gate	40	2Q	11,6
5	1	new	0	cache	15,20,25
5	1	gate	37	2Q	25,20
5	1	gate	39	2Q	20,15
5	2	all2all	0	tensor	32,13,17,18,19,20,21,22,23,24,25,26,27,28,29 ,30,31,32,33,34,35,36,37,38,39,40,41,42,43,44 ,45,46,47,48,4,5,6,7,8,9,10,11,12,13,14 ,15,16
5	2	new	0	cache	32,35,36,40,45
5	2	gate	36	2Q	36,32

Tensor	Phase	Mode	Depth	Gate	Arguments
5	2	gate	37	2Q	40,35
5	2	gate	40	2Q	45,40
5	2	new	0	cache	31,36,41,46
5	2	gate	38	2Q	41,36
5	2	gate	39	2Q	36,31
5	2	gate	40	2Q	46,41
5	2	new	0	cache	27,32,33,37,42
5	2	gate	35	2Q	37,33
5	2	gate	37	2Q	32,27
5	2	gate	38	2Q	42,37
5	2	gate	40	2Q	37,32
5	2	new	0	cache	28,33,34,38,43
5	2	gate	35	2Q	38,34
5	2	gate	37	2Q	43,38
5	2	gate	38	2Q	33,28
5	2	gate	40	2Q	38,33
5	2	new	0	cache	25,29,34,42,47
5	2	gate	38	2Q	34,29
5	2	gate	39	2Q	47,42
5	2	gate	40	2Q	29,25
5	2	new	0	cache	23,27,43,48
5	2	gate	39	2Q	48,43
5	2	gate	39	2Q	27,23
5	2	new	0	cache	24,28,34,39
5	2	gate	39	2Q	39,34
5	2	gate	39	2Q	28,24
5	2	write	0	disk	0,1,2,3,49,50,51,52

The following listing is for the 54-qubit circuit.

Tensor	Phase	Mode	Depth	Gate	Arguments
0	0	define	0	qubits	54
0	0	define	0	disk	0,1,2,3,4,5,6,7,8,23,24,25,26,27,28 ,29,30,31,50,51,52,53
1	1	new	0	tensor	27,0,0,1,2,3,4,5,6,7,8,9,10,11,12 ,13,14,15,16,17,18,19,20,21,22,23,24,25,26
1	1	new	0	cache	10,14,18,19,23
1	1	gate	1	2Q	14,10
1	1	gate	1	2Q	23,19
1	1	gate	3	2Q	18,14
1	1	new	0	cache	2,6,10,18,23
1	1	gate	2	2Q	6,2
1	1	gate	4	2Q	10,6
1	1	new	0	cache	1,5,6,18,23
1	1	gate	2	2Q	5,1
1	1	gate	6	2Q	6,1
1	1	new	0	cache	5,9,14,18,23
1	1	gate	3	2Q	9,5
1	1	gate	6	2Q	14,9
1	1	new	0	cache	0,5,18,23
1	1	gate	5	2Q	5,0
1	1	new	0	cache	18,22,23,26
1	1	gate	2	2Q	26,22
1	1	new	0	cache	18,20,23,24,26
1	1	gate	1	2Q	24,20
1	1	new	0	cache	12,16,18,20,23
1	1	gate	2	2Q	16,12
1	1	gate	4	2Q	20,16
1	1	new	0	cache	18,20,21,23,25
1	1	gate	2	2Q	25,21
1	2	entgl	0	tensor	27,8,0,1,2,3,4,5,6,7,8,9,10,11,12 ,13,14,15,16,17,18,19,20,21,22,23,24,25,26,-1 , -2,-3,-4,-5,-6,-7,-8,-9,-10,-11,-12,-13,-14,-15,-16
1	2	entgl	3	EI	25,-1,-2
1	2	entgl	3	EI	24,-3,-4
1	2	entgl	4	EI	26,-5,-6

Tensor	Phase	Mode	Depth	Gate	Arguments
1	2	entgl	4	EI	23,-7,-8
1	2	new	0	cache	18,20,23,25
1	2	gate	5	2Q	25,20
1	2	gate	6	2Q	23,18
1	2	new	0	cache	11,15,18,23,25
1	2	gate	2	2Q	15,11
1	2	new	0	cache	9,14,15,19,24
1	2	gate	3	2Q	19,15
1	2	gate	5	2Q	24,19
1	2	gate	8	2Q	19,14
1	2	gate	10	2Q	14,9
1	3	entgl	0	tensor	28,13,0,1,2,3,4,5,6,7,8,9,10,11,12 ,13,14,15,16,17,18,19,20,21,22,23,24,25,26,-1 , -2,-3,-4,-5,-6,-7,-8,-9,-10,-11,-12,-13,-14,-15,-16
1	3	entgl	7	EI	24,-9,-10
1	3	entgl	7	EI	23,-11,-12
1	3	entgl	8	EI	25,-15,-16
1	3	new	0	cache	14,18,19,23,24
1	3	gate	9	2Q	24,19
1	3	gate	10	2Q	23,18
1	3	gate	12	2Q	19,14
1	3	new	0	cache	0,5,10,15,20
1	3	gate	6	2Q	15,10
1	3	gate	7	2Q	20,15
1	3	gate	8	2Q	10,5
1	3	gate	9	2Q	5,0
1	3	gate	10	2Q	15,10
1	3	gate	12	2Q	10,5
1	3	new	0	cache	10,14,18,20,25
1	3	gate	9	2Q	25,20
1	3	gate	13	2Q	14,10
1	3	gate	15	2Q	18,14
1	3	new	0	cache	13,15,17,20,21
1	3	gate	1	2Q	17,13
1	3	gate	4	2Q	21,17
1	3	gate	11	2Q	20,15
1	3	new	0	cache	3,7,11,21,26
1	3	gate	1	2Q	7,3
1	3	gate	4	2Q	11,7
1	3	gate	6	2Q	26,21
1	3	new	0	cache	1,5,6,11,16
1	3	gate	5	2Q	16,11
1	3	gate	8	2Q	11,6
1	3	gate	10	2Q	6,1
1	3	gate	14	2Q	5,1
1	3	new	0	cache	0,1,5,9,26
1	3	gate	15	2Q	9,5
1	3	gate	18	2Q	5,1
1	3	gate	19	2Q	9,5
1	3	gate	21	2Q	5,0
1	3	new	0	cache	6,11,15,16,21
1	3	gate	7	2Q	21,16
1	3	gate	9	2Q	16,11
1	3	gate	12	2Q	11,6
1	3	gate	14	2Q	15,11
1	3	new	0	cache	3,4,8,12,13
1	3	gate	1	2Q	8,4
1	3	gate	3	2Q	12,8
1	3	gate	5	2Q	8,3
1	3	gate	7	2Q	13,8
1	3	gate	9	2Q	8,3
1	3	gate	11	2Q	13,8
1	3	gate	13	2Q	8,4
1	3	new	0	cache	2,6,7,12,17
1	3	gate	5	2Q	17,12
1	3	gate	6	2Q	7,2
1	3	gate	7	2Q	12,7
1	3	gate	10	2Q	7,2

Tensor	Phase	Mode	Depth	Gate	Arguments
1	3	gate	14	2Q	6,2
1	3	new	0	cache	6,9,10,14,18
1	3	gate	16	2Q	10,6
1	3	gate	17	2Q	14,10
1	3	gate	19	2Q	18,14
1	3	gate	22	2Q	14,9
1	3	new	0	cache	1,2,6,10,26
1	3	gate	18	2Q	6,2
1	3	gate	20	2Q	10,6
1	3	gate	22	2Q	6,1
1	3	new	0	cache	7,12,13,17,22
1	3	gate	8	2Q	22,17
1	3	gate	9	2Q	17,12
1	3	gate	11	2Q	12,7
1	3	gate	12	2Q	22,17
1	3	gate	13	2Q	17,13
1	3	new	0	cache	3,7,11,21,26
1	3	gate	13	2Q	7,3
1	3	gate	16	2Q	11,7
1	3	gate	17	2Q	7,3
1	4	entgl	0	tensor	30,13,0,1,2,3,4,5,6,7,8,9,10,11,12 ,13,14,15,16,17,18,19,20,21,22,23,24,25,26,-1 ,-2,-3,-4,-5,-6,-7,-8,-9,-10,-11,-12,-13,-14,-15,-16
1	4	entgl	8	EI	26,-13,-14
1	4	new	0	cache	8,12,16,21,26
1	4	gate	10	2Q	26,21
1	4	gate	11	2Q	21,16
1	4	gate	14	2Q	16,12
1	4	gate	15	2Q	12,8
1	4	new	0	cache	4,8
1	4	gate	17	2Q	8,4
2	5	new	0	tensor	27,2,27,28,29,30,31,32,33,34,35,36,37,38,39 ,40,41,42,43,44,45,46,47,48,49,50,51,52,53,-1 ,-2,-3,-4,-5,-6,-7,-8,-9,-10,-11,-12,-13,-14,-15,-16
2	5	new	0	cache	37,41,45,46,50
2	5	gate	1	2Q	50,46
2	5	gate	2	2Q	41,37
2	5	gate	3	2Q	45,41
2	5	gate	6	2Q	50,45
2	5	gate	10	2Q	50,45
2	5	new	0	cache	31,35,38,42,46
2	5	gate	2	2Q	35,31
2	5	gate	2	2Q	42,38
2	5	gate	4	2Q	46,42
2	5	new	0	cache	30,34,35,39,43
2	5	gate	1	2Q	34,30
2	5	gate	1	2Q	43,39
2	5	gate	3	2Q	39,35
2	5	new	0	cache	30,31,35,40,44
2	5	gate	1	2Q	44,40
2	6	entgl	0	tensor	27,6,27,28,29,30,31,32,33,34,35,36,37,38,39 ,40,41,42,43,44,45,46,47,48,49,50,51,52,53,-1 ,-2,-3,-4,-5,-6,-7,-8,-9,-10,-11,-12,-13,-14,-15,-16
2	6	entgl	4	E2Q	30,-5,-6
2	6	entgl	4	E2Q	27,-7,-8
2	6	entgl	8	E2Q	31,-13,-14
2	6	new	0	cache	30,34,35,38,40
2	6	gate	3	2Q	38,34
2	6	gate	6	2Q	35,30
2	6	gate	7	2Q	40,35
2	6	new	0	cache	28,30,32,35,40
2	6	gate	2	2Q	32,28
2	6	new	0	cache	30,32,35,36,40
2	6	gate	4	2Q	36,32
2	6	new	0	cache	36,41,46,47,51
2	6	gate	2	2Q	51,47
2	6	gate	5	2Q	41,36
2	6	gate	6	2Q	51,46

Tensor	Phase	Mode	Depth	Gate	Arguments
2	6	gate	8	2Q	46,41
2	6	gate	9	2Q	41,36
2	6	gate	10	2Q	51,46
2	6	gate	12	2Q	46,41
2	6	new	0	cache	30,35,40,46,50
2	6	gate	13	2Q	50,46
2	6	new	0	cache	27,30,32,35,40
2	6	gate	5	2Q	32,27
2	6	new	0	cache	30,35,40,43,47
2	6	gate	4	2Q	47,43
2	6	new	0	cache	30,35,38,40,43
2	6	gate	6	2Q	43,38
2	7	entgl	0	tensor	27,10,27,28,29,30,31,32,33,34,35,36,37,38,39 ,40,41,42,43,44,45,46,47,48,49,50,51,52,53,-1 ,-2,-3,-4,-5,-6,-7,-8,-9,-10,-11,-12,-13,-14,-15,-16
2	7	entgl	3	E2Q	28,-3,-4
2	7	entgl	8	E2Q	30,-15,-16
2	7	new	0	cache	29,30,33,35,40
2	7	gate	1	2Q	33,29
2	7	gate	10	2Q	35,30
2	7	gate	11	2Q	40,35
2	7	new	0	cache	27,32,33,37,42
2	7	gate	4	2Q	37,33
2	7	gate	6	2Q	42,37
2	7	gate	7	2Q	37,32
2	7	gate	9	2Q	32,27
2	7	new	0	cache	37,42,47,48,52
2	7	gate	2	2Q	52,48
2	7	gate	5	2Q	52,47
2	7	gate	8	2Q	47,42
2	7	gate	9	2Q	52,47
2	7	gate	10	2Q	42,37
2	7	gate	12	2Q	47,42
2	7	new	0	cache	29,32,37,41,45
2	7	gate	11	2Q	37,32
2	7	gate	14	2Q	41,37
2	7	gate	15	2Q	45,41
2	7	new	0	cache	28,33,38,47,51
2	7	gate	5	2Q	33,28
2	7	gate	8	2Q	38,33
2	7	gate	14	2Q	51,47
2	7	new	0	cache	29,34,39,44,48
2	7	gate	3	2Q	48,44
2	7	gate	5	2Q	44,39
2	7	new	0	cache	38,43,48,49,53
2	7	gate	1	2Q	53,49
2	7	gate	5	2Q	53,48
2	7	gate	7	2Q	48,43
2	7	gate	9	2Q	53,48
2	7	gate	10	2Q	43,38
2	7	gate	11	2Q	48,43
2	8	entgl	0	tensor	28,13,27,28,29,30,31,32,33,34,35,36,37,38,39 ,40,41,42,43,44,45,46,47,48,49,50,51,52,53,-1 ,-2,-3,-4,-5,-6,-7,-8,-9,-10,-11,-12,-13,-14,-15,-16
2	8	entgl	3	E2Q	29,-1,-2
2	8	entgl	7	E2Q	28,-11,-12
2	8	new	0	cache	28,33,38,42,46
2	8	gate	9	2Q	33,28
2	8	gate	12	2Q	38,33
2	8	gate	14	2Q	42,38
2	8	gate	16	2Q	46,42
2	8	new	0	cache	46,48,50,52
2	8	gate	14	2Q	52,48
2	8	gate	17	2Q	50,46
2	8	new	0	cache	29,34,39,44,49
2	8	gate	6	2Q	34,29
2	8	gate	7	2Q	49,44
2	8	gate	8	2Q	39,34

Tensor	Phase	Mode	Depth	Gate	Arguments
2	8	gate	9	2Q	44,39
2	8	gate	11	2Q	49,44
2	8	new	0	cache	29,40,44,48,52
2	8	gate	13	2Q	44,40
2	8	gate	15	2Q	48,44
2	8	gate	17	2Q	44,40
2	8	gate	18	2Q	52,48
2	8	gate	19	2Q	48,44
2	8	new	0	cache	29,34,48,49,53
2	8	gate	13	2Q	53,49
2	8	gate	17	2Q	53,49
2	8	gate	21	2Q	53,48
2	9	entgl	0	tensor	30,13,27,28,29,30,31,32,33,34,35,36,37,38,39 ,40,41,42,43,44,45,46,47,48,49,50,51,52,53,-1 ,-2,-3,-4,-5,-6,-7,-8,-9,-10,-11,-12,-13,-14,-15,-16
2	9	entgl	7	E2Q	29,-9,-10
2	9	new	0	cache	29,34,39,43,47
2	9	gate	10	2Q	34,29
2	9	gate	12	2Q	39,34
2	9	gate	13	2Q	43,39
2	9	gate	16	2Q	47,43
2	9	new	0	cache	47,51
2	9	gate	18	2Q	51,47
0	10	slice	0	disk	0,1,2,3,4,50,51,52,53
1	10	all2all	0	tensor	32,6,-1,-2,-3,-4,-5,-6,-7,-8,-9,-10,-11,-12,-13 , -14,-15,-16,11,12,13,14,15,16,17,18,19,20,21,22 ,23,24,25,26,5,6,7,8,9,10
2	10	all2all	0	tensor	32,7,-1,-2,-3,-4,-5,-6,-7,-8,-9,-10,-11,-12,-13 , -14,-15,-16,27,28,29,30,31,32,33,34,35,36,37,38 ,39,40,41,42,43,44,45,46,47,48,49
3	1	new	0	tensor	32,13,11,12,13,14,15,16,17,18,19,20,21,22,23 ,24,25,26,27,28,29,30,31,32,33,34,35,36,37,38 ,39,40,41,42,5,6,7,8,9,10,43,44,45,46,47 ,48,49
3	1	new	0	cache	15,19,23,27,28
3	1	gate	11	2Q	28,23
3	1	gate	13	2Q	23,19
3	1	gate	15	2Q	19,15
3	1	gate	16	2Q	27,23
3	1	gate	17	2Q	23,19
3	1	gate	20	2Q	27,23
3	1	new	0	cache	11,15,18,19,23
3	1	gate	18	2Q	15,11
3	1	gate	19	2Q	19,15
3	1	gate	22	2Q	23,18
3	1	new	0	cache	24,29,33,37,41
3	1	gate	11	2Q	29,24
3	1	gate	13	2Q	33,29
3	1	gate	16	2Q	37,33
3	1	gate	18	2Q	41,37
3	1	new	0	cache	20,24,28,32,36
3	1	gate	13	2Q	24,20
3	1	gate	14	2Q	32,28
3	1	gate	15	2Q	28,24
3	1	gate	16	2Q	36,32
3	1	gate	18	2Q	32,28
3	1	gate	20	2Q	36,32
3	1	new	0	cache	12,16,20,27,32
3	1	gate	16	2Q	20,16
3	1	gate	18	2Q	16,12
3	1	gate	21	2Q	32,27
3	1	new	0	cache	14,19,20,24,28
3	1	gate	17	2Q	24,20
3	1	gate	19	2Q	28,24
3	1	gate	21	2Q	24,19
3	1	gate	24	2Q	19,14
3	1	new	0	cache	16,20,26,31,35
3	1	gate	12	2Q	31,26

Tensor	Phase	Mode	Depth	Gate	Arguments
3	1	gate	14	2Q	35,31
3	1	gate	20	2Q	20,16
3	1	new	0	cache	25,30,34,38,42
3	1	gate	12	2Q	30,25
3	1	gate	13	2Q	34,30
3	1	gate	15	2Q	38,34
3	1	gate	18	2Q	42,38
3	1	new	0	cache	21,25,29,33,37
3	1	gate	14	2Q	25,21
3	1	gate	15	2Q	29,25
3	1	gate	17	2Q	33,29
3	1	gate	20	2Q	37,33
3	1	new	0	cache	18,23,28,33
3	1	gate	21	2Q	33,28
3	1	gate	23	2Q	28,23
3	1	gate	26	2Q	23,18
3	1	new	0	cache	17,20,21,25,29
3	1	gate	16	2Q	21,17
3	1	gate	18	2Q	25,21
3	1	gate	19	2Q	29,25
3	1	gate	21	2Q	25,20
3	1	new	0	cache	22,26,30,34,38
3	1	gate	14	2Q	26,22
3	1	gate	16	2Q	30,26
3	1	gate	17	2Q	34,30
3	1	gate	18	2Q	26,22
3	1	gate	19	2Q	38,34
3	1	gate	20	2Q	30,26
3	1	new	0	cache	19,24,29,34
3	1	gate	22	2Q	34,29
3	1	gate	23	2Q	29,24
3	1	gate	25	2Q	24,19
3	1	new	0	cache	13,17,21,26
3	1	gate	17	2Q	17,13
3	1	gate	20	2Q	21,17
3	1	gate	22	2Q	26,21
3	1	new	0	cache	26,31,35,39
3	1	gate	15	2Q	39,35
3	1	gate	18	2Q	35,31
3	1	gate	24	2Q	31,26
3	2	all2all	0	tensor	32,13,18,19,20,21,22,23,24,25,26,27,28,29,30 ,31,32,33,34,35,36,37,38,39,40,41,42,43,44,45 ,46,47,48,49,5,6,7,8,9,10,11,12,13,14,15 ,16,17
3	2	new	0	cache	27,32,37,42,46
3	2	gate	20	2Q	46,42
3	2	gate	22	2Q	42,37
3	2	gate	23	2Q	37,32
3	2	gate	25	2Q	32,27
3	2	new	0	cache	33,38,39,43,47
3	2	gate	17	2Q	43,39
3	2	gate	20	2Q	47,43
3	2	gate	22	2Q	43,38
3	2	gate	24	2Q	38,33
3	2	new	0	cache	28,33,38,43,48
3	2	gate	23	2Q	48,43
3	2	gate	25	2Q	33,28
3	2	gate	26	2Q	43,38
3	2	gate	28	2Q	38,33
3	2	new	0	cache	23,28,30,35,39
3	2	gate	19	2Q	39,35
3	2	gate	22	2Q	35,30
3	2	gate	27	2Q	28,23
3	2	new	0	cache	29,34,39,44,49
3	2	gate	21	2Q	44,39
3	2	gate	23	2Q	49,44
3	2	gate	24	2Q	39,34
3	2	gate	25	2Q	44,39

Tensor	Phase	Mode	Depth	Gate	Arguments
3	2	gate	26	2Q	34,29
3	2	gate	27	2Q	49,44
3	2	gate	28	2Q	39,34
3	2	new	0	cache	24,25,29,30,33
3	2	gate	24	2Q	30,25
3	2	gate	27	2Q	29,24
3	2	gate	29	2Q	33,29
3	2	new	0	cache	30,35,40,44
3	2	gate	23	2Q	40,35
3	2	gate	26	2Q	35,30
3	2	gate	27	2Q	40,35
3	2	gate	29	2Q	44,40
3	2	new	0	cache	36,41,45
3	2	gate	19	2Q	45,41
3	2	gate	21	2Q	41,36
3	3	all2all	0	tensor	32,13,5,6,7,8,9,10,11,12,13,14,15,16,17 ,18,19,20,21,22,23,24,25,26,27,28,29,30,31,32 ,33,34,35,36,37,38,39,40,41,42,43,44,45,46,47 ,48,49
3	3	new	0	cache	9,14,19,23,27
3	3	gate	26	2Q	14,9
3	3	gate	28	2Q	19,14
3	3	gate	29	2Q	23,19
3	3	gate	32	2Q	27,23
3	3	new	0	cache	10,15,20,25,30
3	3	gate	22	2Q	15,10
3	3	gate	23	2Q	20,15
3	3	gate	25	2Q	25,20
3	3	gate	28	2Q	30,25
3	3	new	0	cache	5,10,15,30,34
3	3	gate	24	2Q	10,5
3	3	gate	26	2Q	15,10
3	3	gate	29	2Q	34,30
3	3	new	0	cache	7,11,15,20,24
3	3	gate	20	2Q	11,7
3	3	gate	27	2Q	20,15
3	3	gate	29	2Q	24,20
3	3	new	0	cache	11,16,21,26,31
3	3	gate	21	2Q	16,11
3	3	gate	23	2Q	21,16
3	3	gate	26	2Q	26,21
3	3	gate	28	2Q	31,26
3	3	new	0	cache	6,11,16,31,35
3	3	gate	24	2Q	11,6
3	3	gate	25	2Q	16,11
3	3	gate	30	2Q	35,31
3	3	new	0	cache	16,21,25,29
3	3	gate	27	2Q	21,16
3	3	gate	30	2Q	25,21
3	3	gate	31	2Q	29,25
3	3	new	0	cache	8,12,17,22
3	3	gate	19	2Q	12,8
3	3	gate	21	2Q	17,12
3	3	gate	24	2Q	22,17
3	3	write	0	disk	0,1,2,3,4,50,51,52,53
4	1	read	0	disk	23,24,25,26,27,28,29,30,31
4	1	new	0	tensor	32,13,0,1,2,3,4,5,6,7,8,9,10,11,12 ,13,14,15,16,17,18,19,20,21,22,32,33,34,35,36 ,37,38,39,40,41,42,43,44,45,46,47,48,49,50,51 ,52,53
4	1	new	0	cache	0,5,10,14,18
4	1	gate	25	2Q	5,0
4	1	gate	28	2Q	10,5
4	1	gate	29	2Q	14,10
4	1	gate	31	2Q	18,14
4	1	new	0	cache	0,1,5,6,9
4	1	gate	26	2Q	6,1
4	1	gate	30	2Q	5,1

Tensor	Phase	Mode	Depth	Gate	Arguments
4	1	gate	31	2Q	9,5
4	1	gate	34	2Q	5,1
4	1	gate	35	2Q	9,5
4	1	gate	37	2Q	5,0
4	1	new	0	cache	6,11,15,19
4	1	gate	28	2Q	11,6
4	1	gate	30	2Q	15,11
4	1	gate	31	2Q	19,15
4	1	new	0	cache	2,6,7,10,12
4	1	gate	22	2Q	7,2
4	1	gate	23	2Q	12,7
4	1	gate	26	2Q	7,2
4	1	gate	30	2Q	6,2
4	1	gate	32	2Q	10,6
4	1	gate	34	2Q	6,2
4	1	new	0	cache	6,9,10,14,18
4	1	gate	33	2Q	14,10
4	1	gate	35	2Q	18,14
4	1	gate	36	2Q	10,6
4	1	gate	38	2Q	14,9
4	1	new	0	cache	1,6,12,17,22
4	1	gate	25	2Q	17,12
4	1	gate	28	2Q	22,17
4	1	gate	38	2Q	6,1
4	1	new	0	cache	3,8,13,17,21
4	1	gate	21	2Q	8,3
4	1	gate	23	2Q	13,8
4	1	gate	25	2Q	8,3
4	1	gate	27	2Q	13,8
4	1	gate	29	2Q	17,13
4	1	gate	32	2Q	21,17
4	1	gate	33	2Q	17,13
4	1	new	0	cache	3,7,11,12,15
4	1	gate	27	2Q	12,7
4	1	gate	29	2Q	7,3
4	1	gate	32	2Q	11,7
4	1	gate	33	2Q	7,3
4	1	gate	34	2Q	15,11
4	1	gate	36	2Q	11,7
4	1	new	0	cache	2,7,12,16,20
4	1	gate	30	2Q	16,12
4	1	gate	32	2Q	20,16
4	1	gate	38	2Q	7,2
4	1	new	0	cache	3,4,8,12,16
4	1	gate	29	2Q	8,4
4	1	gate	31	2Q	12,8
4	1	gate	33	2Q	8,4
4	1	gate	34	2Q	16,12
4	1	gate	35	2Q	12,8
4	1	gate	37	2Q	8,3
4	1	new	0	cache	8,13
4	1	gate	39	2Q	13,8
4	2	all2all	0	tensor	32,13,13,14,15,16,17,18,19,20,21,22,32,33,34 ,35,36,37,38,39,40,41,42,43,44,45,46,47,48,49 ,50,51,52,53,0,1,2,3,4,5,6,7,8,9,10 ,11,12
4	2	new	0	cache	39,43,48,49,53
4	2	gate	25	2Q	53,48
4	2	gate	27	2Q	48,43
4	2	gate	29	2Q	43,39
4	2	gate	29	2Q	53,49
4	2	gate	33	2Q	53,49
4	2	new	0	cache	42,44,47,48,52
4	2	gate	21	2Q	52,47
4	2	gate	24	2Q	47,42
4	2	gate	25	2Q	52,47
4	2	gate	30	2Q	52,48
4	2	gate	31	2Q	48,44

Tensor	Phase	Mode	Depth	Gate	Arguments
4	2	gate	34	2Q	52,48
4	2	new	0	cache	40,44,48,53
4	2	gate	33	2Q	44,40
4	2	gate	35	2Q	48,44
4	2	gate	37	2Q	53,48
4	2	new	0	cache	34,37,38,42,47
4	2	gate	26	2Q	42,37
4	2	gate	28	2Q	47,42
4	2	gate	30	2Q	42,38
4	2	gate	31	2Q	38,34
4	2	new	0	cache	41,43,46,47,51
4	2	gate	22	2Q	51,46
4	2	gate	24	2Q	46,41
4	2	gate	26	2Q	51,46
4	2	gate	30	2Q	51,47
4	2	gate	32	2Q	47,43
4	2	gate	34	2Q	51,47
4	2	new	0	cache	35,39,43,47,52
4	2	gate	31	2Q	39,35
4	2	gate	33	2Q	43,39
4	2	gate	36	2Q	47,43
4	2	gate	37	2Q	52,47
4	2	new	0	cache	32,36,37,41,46
4	2	gate	25	2Q	41,36
4	2	gate	27	2Q	37,32
4	2	gate	28	2Q	46,41
4	2	gate	30	2Q	41,37
4	2	new	0	cache	38,42,45,46,50
4	2	gate	22	2Q	50,45
4	2	gate	26	2Q	50,45
4	2	gate	29	2Q	50,46
4	2	gate	32	2Q	46,42
4	2	gate	33	2Q	50,46
4	2	gate	34	2Q	42,38
4	2	gate	36	2Q	46,42
4	2	new	0	cache	33,37,41,45,50
4	2	gate	31	2Q	45,41
4	2	gate	32	2Q	37,33
4	2	gate	34	2Q	41,37
4	2	gate	35	2Q	45,41
4	2	gate	38	2Q	50,45
4	2	new	0	cache	46,51
4	2	gate	38	2Q	51,46
4	2	write	0	disk	23,24,25,26,27,28,29,30,31
5	1	read	0	disk	0,1,2,3,4,50,51,52,53
5	1	new	0	tensor	32,13,5,6,7,8,9,10,11,12,13,14,15,16,17 ,18,19,20,21,22,23,24,25,26,27,28,29,30,31,32 ,33,34,35,36,37,38,39,40,41,42,43,44,45,46,47 ,48,49
5	1	new	0	cache	5,10,15,19,23
5	1	gate	33	2Q	23,19
5	1	gate	35	2Q	19,15
5	1	gate	38	2Q	15,10
5	1	gate	40	2Q	10,5
5	1	new	0	cache	7,12,17,21,25
5	1	gate	34	2Q	25,21
5	1	gate	36	2Q	21,17
5	1	gate	37	2Q	17,12
5	1	gate	39	2Q	12,7
5	1	new	0	cache	17,22,26,30,34
5	1	gate	30	2Q	26,22
5	1	gate	32	2Q	30,26
5	1	gate	33	2Q	34,30
5	1	gate	34	2Q	26,22
5	1	gate	36	2Q	30,26
5	1	gate	40	2Q	22,17
5	1	new	0	cache	21,26,31,35
5	1	gate	34	2Q	35,31

Tensor	Phase	Mode	Depth	Gate	Arguments
5	1	gate	38	2Q	26,21
5	1	gate	40	2Q	31,26
5	1	new	0	cache	18,23,27,29,33
5	1	gate	33	2Q	33,29
5	1	gate	36	2Q	27,23
5	1	gate	38	2Q	23,18
5	1	new	0	cache	24,27,28,32,36
5	1	gate	30	2Q	32,28
5	1	gate	31	2Q	28,24
5	1	gate	32	2Q	36,32
5	1	gate	34	2Q	32,28
5	1	gate	36	2Q	36,32
5	1	gate	37	2Q	32,27
5	1	new	0	cache	14,19,20,24,28
5	1	gate	33	2Q	24,20
5	1	gate	35	2Q	28,24
5	1	gate	37	2Q	24,19
5	1	gate	40	2Q	19,14
5	1	new	0	cache	6,11,16,20,21
5	1	gate	36	2Q	20,16
5	1	gate	37	2Q	16,11
5	1	gate	39	2Q	21,16
5	1	gate	40	2Q	11,6
5	1	new	0	cache	15,20,25,29
5	1	gate	35	2Q	29,25
5	1	gate	37	2Q	25,20
5	1	gate	39	2Q	20,15
5	2	all2all	0	tensor	32,13,18,19,20,21,22,23,24,25,26,27,28,29,30 ,31,32,33,34,35,36,37,38,39,40,41,42,43,44,45 ,46,47,48,49,5,6,7,8,9,10,11,12,13,14,15 ,16,17
5	2	new	0	cache	33,36,37,41,46
5	2	gate	36	2Q	37,33
5	2	gate	37	2Q	41,36
5	2	gate	40	2Q	46,41
5	2	new	0	cache	32,37,42,47
5	2	gate	38	2Q	42,37
5	2	gate	39	2Q	37,32
5	2	gate	40	2Q	47,42
5	2	new	0	cache	28,33,34,38,43
5	2	gate	35	2Q	38,34
5	2	gate	37	2Q	33,28
5	2	gate	38	2Q	43,38
5	2	gate	40	2Q	38,33
5	2	new	0	cache	29,34,35,39,44
5	2	gate	35	2Q	39,35
5	2	gate	37	2Q	44,39
5	2	gate	38	2Q	34,29
5	2	gate	40	2Q	39,34
5	2	new	0	cache	25,30,35,43,48
5	2	gate	38	2Q	35,30
5	2	gate	39	2Q	48,43
5	2	gate	40	2Q	30,25
5	2	new	0	cache	23,28,44,49
5	2	gate	39	2Q	49,44
5	2	gate	39	2Q	28,23
5	2	new	0	cache	24,29,35,40
5	2	gate	39	2Q	40,35
5	2	gate	39	2Q	29,24
5	2	write	0	disk	0,1,2,3,4,50,51,52,53